1-1-2016

Interactions of Organodithiols with Gold and Silver Nanoparticles in Water

Manuel Gadogbe

Interactions of organodithiols with gold and silver nanoparticles in water

By

Manuel Gadogbe

A Dissertation
Submitted to the Faculty of
Mississippi State University
in Partial Fulfillment of the Requirements
for the Degree of Doctor of Philosophy
in Chemistry
in the Department of Chemistry

Mississippi State, Mississippi

May 2016

Interactions of organodithiols with gold and silver nanoparticles in water

By

Manuel Gadogbe

Approved:

_____

Dongmao Zhang
(Major Professor)

_____

David O. Wipf
(Committee Member)

_____

Todd E. Mlsna
(Committee Member)

_____

Joseph P. Emerson
(Committee Member)

_____

Stephen C. Foster
(Graduate Coordinator and Committee Member)

_____

Rick Travis
Interim Dean
College of Arts & Sciences

Name: Manuel Gadogbe

Date of Degree: May 7, 2016

Institution: Mississippi State University

Major Field: Chemistry

Major Professor: Dongmao Zhang

Title of Study: Interactions of organodithiols with gold and silver nanoparticles in water

Pages in Study 90

Candidate for Degree of Doctor of Philosophy

Organodithiols including para-aryl dithiols (PADTs, HS-$(C_6H_4)_n$-SH, n = 1, 2 and 3) and alpha, omega-alkanedithiols (ADTs, HS-$(CH_2)_n$-SH, n = 2, 4, …) with two distal thiols have been used extensively in molecular electronics, surface-enhanced Raman spectroscopy (SERS), and quantum electron tunneling between two gold or silver nanoparticles (AuNPs and AgNPs). The popular belief is that these dithiols cross-link noble metal nanoparticles (NPs) as monolayer dithiolate spacers. Reported is the finding that PADTs predominantly exist as monothiolate forms on AuNPs or AgNPs. No PADT-induced NP cross-linking was observed regardless of NP/PADT concentration ratios. 1,4-benzenedimethanethiol (HS-CH_2-(C_6H_4)-CH_2-SH) and ADT can be completely deprotonated, forming dithiolates on AuNPs and AgNPs, while only one PADT thiol can be deprotonated even when PADTs are treated with concentrated NaOH or $AgNO_3$. AuNP localized surface plasmon resonance (LSPR) measurement provides conclusive evidence that ADT in AuNP junctions primarily consisted of dithiolate monomers in which the two sulfides are either attached to the same AuNP, or cross-link two adjacent AuNPs as single-molecular spacers. However, ADT molecules most likely in the area surrounding the AuNP junction are monothiolate with their distal thiols either remaining

intact or forming disulfide cross-links with neighboring adsorbed ADTs. The possibility for ADT to cross-link two AgNPs as single molecular linker is excluded on the basis of TEM measurements that showed ADT-induced AgNP disintegration. This work highlights the difference between organothiol interactions with AgNPs and AuNPs and should be of broad importance for plasmonic NP research given the popularity of PADTs in molecular electronics and SERS applications.

DEDICATION

I would like to dedicate this doctoral dissertation to my lovely wife Juliet Gadogbe and my late mother Christine Aku Nedzro for their love, enormous support, and for adding meaning to my life.

ACKNOWLEDGEMENTS

This dissertation “emerged” from the collective help, support, and direction of many wonderful people without whose assistance and help this journey would have never been a successful one. I would like to particularly acknowledge several people.

First and foremost, I am deeply indebted to my advisor Dr. Dongmao Zhang, without whose scientific expertise, strategic direction, and mentoring, I would not have gotten this far. I consider it truly a privilege to have worked in such an encouraging and academically engaging environment.

I am grateful to all of my committee members Dr. Stephen C. Foster, Dr. David O. Wipf, Dr. Joseph P. Emerson, Dr. Todd E. Mlsna and my former committee member Dr. Svein Saebø for their helpful suggestions and discussions. I sincerely thank the graduate coordinator, Dr. Stephen C. Foster, for his guidance throughout my graduate career.

I want to thank all our collaborators: Dr. Shengli Zou (University of Central Florida), Yadong Zhou (University of Central Florida), Dr. Maodu Chen (Dalian University of Technology), Xiuming Zhao (Dalian University of Technology), and Dr. Charles U. Pittman, Jr. (Mississippi State University). I thank them all for their insightful input, advice, and valuable discussions.

I also wish to express my sincere gratitude to Dr. Willard Collier, Dr. Svein Saebø, and Dr. Debbie J. Beard for the editorial assistance on writing my manuscripts and dissertation.

I would also like to thank current and past co-workers of Dr. Zhang's lab who have been friendly, open-minded, and supportive friends in my journey.

Finally, my most heartfelt acknowledgment goes to my wife who has been a strong pillar behind me all throughout this challenging journey and without whose selfless sacrifices, I wouldn't have come this far.

.

TABLE OF CONTENTS

LIST OF TABLES

LIST OF FIGURES

LIST OF ABBREVIATIONS

NPs	Nanoparticles
AuNPs	Gold nanoparticles
AgNPs	Silver nanoparticles
SERS	Surface enhanced Raman spectroscopy
SAM	Self-assembled monolayer
PADTs	Para-aryl dithiols
ADTs	α,ω-alkanedithiols
XPS	X-ray photoelectron spectroscopy
FT-IR	Fourier transform infrared spectroscopy
RAIRS	Reflection-absorption infrared spectroscopy
TOF-DRS	Direct recoil spectroscopy with time of flight
TEM	Transmission electron microscopy
UV-vis	Ultraviolet visible
BDMT	1,4-benzenedimethanethiol
BDT	1,4- benzenedithiol
LSPR	Localized surface plasmon resonance
EM	Electromagnetic
CE	Chemical enhancement
EDT	1, 2-ethanedithiol

BPDT	Biphenyl-4,4'-dithiol
TPDT	*p*-terphenyl-4,4"-dithiol
DFT	Density functional theory
NA	Numerical aperture of objective
ICP-MS	Inductively-coupled plasma mass-spectrometry
PrDT	1,3-propanedithiol
BuDT	1,4-butanedithiol
HDT	1,6-hexanedithiol
AMTs	Alkylmonothiols
ME	Mercaptoethanol
HED	2-hydroxyethyldisulfide
DRC	Dynamic reaction cell
BuT	1-butanethiol

CHAPTER I

INTRODUCTION

Noble metal nanoparticles (NPs) have attracted significant attention because of their importance in a number of fields such as biosensing, catalysis, drug delivery, solar cells, and surface enhanced Raman spectroscopy (SERS).[1-11] Their use in these applications stems from the fact that noble metal NPs have unique chemical and electromagnetic properties. The physical and chemical properties of metal NPs differ from those of their constituent atoms or the metals in the bulk form. For example, bulk gold is unreactive while gold nanoparticles (AuNPs) can be catalytically active.[12] Also, gold in the bulk state is yellow while AuNPs are red or pink in color and bulk silver is metallic while silver nanoparticles (AgNPs) are pale yellow.

The most extensively studied metal NP systems are AuNPs and AgNPs.[12] Compared to AgNPs however, AuNPs are more extensively studied due to the ease of obtaining monodispersity in their particle sizes and well defined control over their shape.

The most common method of AuNP synthesis is the citrate reduction method first developed by Turkevich in 1951.[13] This method is used to synthesize stable AuNPs in water and involves the reduction of chloroaurate ($AuCl_4^-$) using sodium citrate. AuNPs of approximately 20 nm in diameter are produced by using this method. By varying the ratio of the $AuCl_4^-$ to citrate, Frens, in 1973, successfully obtained AuNPs in the size range of 16 – 150 nm.[14] In the Turkevich method, the citrate acts both as the reducing agent and

capping agent to impart dispersion stability to the AuNPs in water. This dispersion stability of the AuNPs is achieved due to electrostatic repulsion between the negative surface charges from adsorbed citrate on the AuNPs.[15] Another method for synthesizing AuNPs is the two phase Brust-Schiffrin method which involves the reduction of the $AuCl_4^-$ with citrate or sodium borohydride in the presence of thiol as the capping agent.[16] Unlike the Turkevich method, the Brust-Schiffrin synthesis produces only small NPs (1 – 3 nm). The AuNPs can be redissolved in organic solvents.[16, 17] Because of the small size of the NPs and the monolayer of thiols that are formed during the synthesis, they are called monolayer protected clusters (MPCs).[12]

On the other hand, the most common method of AgNPs synthesis is the citrate reduction method developed by Lee and Misel in 1982.[18] This method involves the reduction of $AgNO_3$ using sodium citrate as the reducing agent. This approach leads to formation of citrate-stabilized colloidal AgNPs (in the size range between 50-100 nm) in water.[19] A major disadvantage of this method however, is that the NP size distribution is not narrow. Reduction with sodium borohydride also leads to the formation of smaller NPs. A less common approach of synthesizing AgNPs also involves γ-irradiation of a solution of silver salt (e.g. $AgClO_4$ or $AgNO_3$) in the presence of citrate as the stabilizing agent and an alcohol as a radical scavenger. This method typically leads to the formation of AgNPs in the size range of 5-20 nm.[19, 20]

The majority of noble metal NP applications require functionalization of the NP surface. For example, in delivery applications, drugs are anchored with thiol linkers onto the NP surface taking advantage of thiols' high affinity for AuNPs and AgNPs. Surface functionalization imparts stability, functionality, and target specificity (e.g. in sensing and

drug delivery applications) to the NPs. Understanding the interfacial interaction and structure and or conformation of molecules on the NP surfaces is therefore an important aspect of NP research because the structure/conformation determines the physical, chemical, and biological properties.

1.1 Surface functionalization of AuNPs and AgNPs

Noble metal NPs can be functionalized with various organic and biomolecules. Surface functionalization is a way of tuning the interfacial properties of the NP for its specific application. Surface functionalization requires that the adsorbates can be easily attached to the NP surface. The ideal molecule for functionalization should be one that has a high affinity for the surface of interest and can displace adventitious adsorbates on the NP surface. Self-assembled monolayers (SAMs) provide a good platform to tune the interfacial properties of NPs. SAMs are ordered monolayers of organic assemblies formed as a result of spontaneous adsorption of molecules from solution or gas phase onto the surface of planar metal films or metal NPs.[21]

Three approaches can be used in the surface functionalization of NPs. First, the NPs can be functionalized with the ligands of interest during the NP synthesis process. An example of this is in the Brust-Schiffrin synthesis where the functionalizing ligands (thiols) are directly added during the synthesis.[16] The second approach involves addition of the ligand after the synthesis of the NPs. In this case, the ligand should have the ability to displace the capping ligand on the NP during synthesis and form a covalent bond with the surface. An example of this, is the functionalization of citrate-capped AuNPs using thiols.[22] The third approach is through specific conjugation of an already existing covalently attached adsorbate to an incoming ligand.[23]

The most extensively used molecules for surface functionalization of AuNPs and AgNPs are organothiols (organic molecules with thiol functional groups). This is because of the high affinity of thiol groups for AuNPs and AgNPs. For example, gold is known to form relatively strong Au-thiolate bonds (~ 40 kcal/mol).[21, 24]

SAMs on Au and Ag surfaces are also easy to prepare. A typical procedure for preparing SAMs involves the immersion or incubation of the substrates in freshly prepared dilute solutions (micromolar to millimolar concentrations) of organothiols for approximately 12-18 h at room temperature. Adsorption of the organothiols onto the substrates is usually fast (from few seconds to minutes) forming ~ 80-90% of the monolayer followed by a slow reorganization of the chains which could take several hours. Other experimental factors such as the solvent, temperature, immersion time, purity of the organothiol, oxygen content of the solution, and chain length of the adsorbate may affect the formation kinetics and structure of the SAM.[21, 25]

The interaction and structure of alkanethiols on planar gold and silver films as well as NPs has been studied extensively,[25-33] however, organodithiols are also attracting much attention in the literature because of their utility in molecular electronics, SERS, and fabrication of high order nanostructures.[34-36]

1.2 Organodithiols interactions with AuNPs and AgNPs

Organodithiols are an important class of organothiols that are gaining attention in the literature. Unlike monothiols that have only one thiol (-SH) group, organodithiols possess two –SH groups. The fact that two –SH groups exist in organodithiols introduces some complexity in their interactions with Au and Ag surfaces since they may exist as

monothiolates in which only one of the two –SH groups is deprotonated or as dithiolates in which both –SH groups are deprotonated.

Adsorption of alkanethiols onto Au and Ag surfaces is well understood. It is generally accepted that alkanethiol adsorption involves an intial fast adsorption with the alkanethiols in a "lying down" configuration followed by slow chain reorganization from the "lying down" to the "standing up" configuration. In the case of dithiols however, this transition from "lying down" to "standing up" configuration can be hindered when there is the formation of two Au-thiolate bonds and this transition is not well understood. Nevertheless, highly ordered SAMs of dithiols on Au and Ag surfaces are also observed indicating the possibility of such a transition.[37, 38] In the case of dithiols, a "standing up" configuration will imply that the dithiols are anchored to the Au or Ag surface through a single Au-S or Ag-S bond, while the "lying down" configuration will involve the formation of two Au-S or Ag-S bonds.

Studies involving the interaction of organodithiols with planar gold and silver films as well as NPs exist as discussed in the next section. However, studies on NP systems are limited compared to studies on planar films. The structure of SAMs can differ greatly depending on the curvature and defects on the surface. As such the interaction of organothiols and organodithiols with planar films cannot provide detailed information about their interaction with NPs which have surface curvatures and surface defects.

Of particular interest among the organodithiols, para-aryl dithiols (PADTs) and α,ω-alkanedithiols (ADTs) have received major attention in the plasmonic NP research community because of their widespread utility in molecular electronics, and SERS

applications where they are generally believed to act as single molecule dithiolate linkers. However, detailed studies of the interaction of these dithiols with plasmonic NPs have been quite limited. This work will focus on the study of the interactions of the aforementioned two classes of organodithiols with AuNPs and AgNPs in water in an attempt to gain deeper insight into their structure and orientation on these surfaces.

1.3 Analytical methods for studying organodithiols interactions with Au and Ag surfaces

Various analytical tools exist for characterizing SAMs of dithiols on planar films and NPs. The choice of specific tools depends on the type and details of information being sought about the SAM, the resolution of the analytical technique, and also the type of substrate. The adsorption and structures of organodithiols on Au and Ag films have been characterized by X-ray photoelectron spectroscopy (XPS),[38-45] Fourier transform infrared spectroscopy (FT-IR),[43] ellipsometry,[46] reflection-absorption infrared spectroscopy (RAIRS),[41, 47] cyclic voltammetry,[43, 48] and direct recoil spectroscopy with time of flight (TOF-DRS).[49, 50]

"Standing up" monothiolate and well-ordered SAMs of 1,4-benzenedimethanethiol (BDMT) with a free pendant –SH group were reported for BDMT adsorption from solution phase onto Au film characterized by RAIRS, XPS, and ellipsometry.[51, 52] Using XPS, and TOF-DRS, Jia et al. and Alarcón et al. independently reported that gas phase adsorption of BDMT on Au and Ag films results in a lying down phase at low exposures and a standing up phase at high exposures.[45, 50] Stammer et al. reported that the dithiol molecule 2-mercaptomethylbenzenethiol, adsorbs as a dithiolate on Au based on the absence of the –SH stretch in their RAIRS spectrum.[41]

The structures of organodithiols on AuNP and AgNP systems have also been characterized using XPS and vibrational spectroscopic techniques such as FT-IR, and SERS.[48, 53-56] On the basis of their FT-IR measurements, Pradeep et al. reported that BDMT forms flat lying dithiolates on 3 nm Au and Ag nanoclusters in which two Au-S or Ag-S bonds are formed. This conclusion was based on the disappearance of the –SH stretching vibrations in the FT-IR spectrum.[57] From their SERS measurements, Cho et al. believed that 1,4-benzenedithiol (BDT) exists as a dithiolate both in basic solution and on AgNPs due to the apparent disappearance of the –SH peak.[55]

XPS is an important technique for characterizing surface molecules. It provides information about the elemental composition of the surface as well as the charge states of the species adsorbed onto the surfaces. However, it also suffers from several disadvantages such as X-ray induced damage to the surface molecules,[58, 59] which could lead to misleading results and incorrect conclusions about the structure and composition of the SAMs. In addition, it is difficult to resolve peaks associated with thiol (S-H) and disulfide (S-S) in XPS because they have the same binding energies (~163.5 eV).[42] This limitation is not encountered in SERS since SERS has the advantage of resolving –SH and S-S peaks which appear at different wavenumbers (~2600 cm^{-1} and ~520 cm^{-1} respectively) in the acquired spectrum.

Vibrational techniques such as IR and SERS are particularly useful for the study of the orientation of molecules adsorbed on the surfaces of metal NPs based on their surface selection rules.[60-62] Combining these techniques with theoretical calculations, enables reliable information to be obtained about molecular orientation of adsorbed molecules on AuNPs and AgNPs. Even though IR has several advantages over other

experimental methods (e.g. XPS) such as less tedious experimental procedures during spectral acquisition, it is also limited in certain respects such as sensitivity and spectral interference from solvents.

On the other hand, SERS is a very sensitive technique for the study of the interfacial structure and adsorption mechanism of molecules adsorbed onto AuNPs and AgNPs even at submonolayer concentration of adsorbates.[63] The high sensitivity of SERS towards the determination of adsorbed molecules is due to the strong electromagnetic enhancement that is experienced by the molecules adsorbed onto the AuNP or AgNP surfaces.[9, 64]

The interaction of molecules with AuNPs and AgNPs can also be qualitatively monitored in-situ using UV-vis spectroscopy by taking advantage of the unique optical property of these NPs called the localized surface plasmon resonance (LSPR) which depends on factors such as the size, shape, and dielectric environment of the NPs.[65, 66] Since the adsorption of molecules onto AuNPs and AgNPs mostly leads to a change in the dielectric environment immediately surrounding the NPs, the LSPR of the NPs can be qualitatively monitored during these interactions. While the use of UV-vis spectroscopy is simple and fast, this can only provide qualitative information about the system. In this work, we took advantage of the high sensitivity provided by SERS and the LSPR associated with these NPs to develop an insight into the interaction of organodithiols with AuNPs and AgNPs in water.

The following sections provide information about the fundamental principles governing the LSPR and SERS which have been largely employed in this study.

1.4 Localized Surface Plasmon Resonance (LSPR)

AuNPs and AgNPs exhibit a strong optical resonance phenomenon called LSPR when they interact with light. The LSPR of NPs is due to resonant collective oscillation of the conduction electrons of the NPs with the frequency of the incident light. As a result, AuNPs and AgNPs exhibit strong extinction (absorption and scattering) in the UV-visible region. The spectrum thus obtained is called the LSPR spectrum.[67-69] Figure 1.1 shows the schematic representation of the surface plasmon oscillation for spherical NPs.[65]

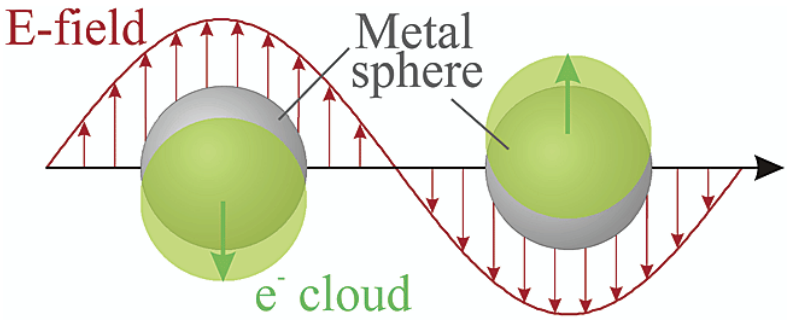

Figure 1.1 Schematic representation of surface plasmon oscillation of spherical NPs. Reproduced from ref 60.

The LSPR spectra of NPs depend on several factors such as the size, shape, and dielectric environment and aggregation state of the NPs.[65, 66, 70] For example 13 nm citrate-capped AuNPs have extinction peak maximum in the LSPR spectrum at ~520 nm while a 50 nm citrate-capped AuNPs have the maximum typically at ~540 nm. The LSPR of NPs (e.g. 10-100 nm) increases with the particle size because of the increase in the extinction coefficient of the NPs.[65] This particle size dependence of the LSPR is explained using the Mie theory (equation 1.1)[68, 71, 72]

$$C_\lambda = \frac{24\varepsilon^2 R^3 \varepsilon_{out}^{3/2}}{\lambda}\left[\frac{\varepsilon_2}{(\varepsilon_1+2\varepsilon_{out})^2+\varepsilon_2^2}\right] \quad (1.1)$$

Where;

C_λ is extinction cross section for the NP.

λ is the wavelength of the electromagnetic wave.

R is radius of the NP.

ε_{out} is the dielectric function of the medium surrounding the NP.

ε_1 and ε_2 are dielectric constants of real and imaginary parts of the NP respectively.

LSPR is also sensitive to the proximity of NPs. Thus, aggregation of NPs will result in the red shift of the LSPR band as the solution turns from red to blue due to the plasmon coupling between neighboring NPs.[73]

This plasmon coupling between NPs also leads to an increase in the electric field generated between the NPs. The enhanced electromagnetic field generated is the cause of the strong signals generated for molecules on the NPs in SERS.[68]

1.5 Surface enhanced Raman Spectroscopy (SERS)

The low efficiency of inelastic scattering of photons by a molecule in Raman spectroscopy makes the direct sensitive detection of analytes in Raman spectroscopy difficult. In the presence of plasmonic NPs such as AuNPs and AgNPs, strong Raman signal intensities have been observed in several experiments with enhancements up to 10^6 orders of magnitude.[9, 64] This phenomenon was attributed to the electromagnetic enhancement induced at the surface of the NPs in the presence of light and is referred to

as surface enhanced Raman scattering, thus giving birth to the technique, surface enhanced Raman spectroscopy (SERS). The large enhancements in the Raman signal generated has made SERS a powerful analytical technique for studying ligand adsorption onto AuNPs and AgNPs taking advantage of its single molecule detection sensitivity and the fact that fingerprint spectra of analytes can be obtained.[74, 75] In addition, measurements can be done in an aqueous environment.

Two main mechanisms have been accepted as the underlying mechanisms causing the enhancement of the SERS signals. These are the electromagnetic (EM) enhancement, which occurs due to the resonances of the incident electromagnetic field with the surface plasmons of the metal NPs as discussed above,[76] and chemical enhancement (CE). CE is mostly due to charge transfer interactions of adsorbed molecules with the metal NPs.[77, 78] The major part of the enhancement observed in SERS is due to the EM enhancement ($\geq 10^4$) while CE is known to provide an order or two of magnitude in enhancement to the Raman signal intensity.[76-78]

Interaction of an external field (E_o) with a small spherical NP induces an electromagnetic field ($E_{induced}$) at the surface of the NP. The field induced at the surface of the sphere is related to the applied external field by the following equation;[76]

$$E_{induced} = [\frac{\varepsilon_{1(\omega)} - \varepsilon_3}{\varepsilon_1(\omega) + 2\varepsilon_3}]E_O \quad (1.2)$$

Where $\varepsilon_1(\omega)$ is the frequency dependent dielectric function of the metal.

ε_3 is the relative permittivity of the ambient phase.

The EM enhancement becomes even higher at gaps between NPs that are very close to each other due to their plasmon coupling. Indeed, it has been shown that reducing

the interparticle distance increases the Raman signal of molecules at these interparticle gaps.[79] In practical SERS measurements, the generation of these gaps is induced by adding electrolytes to the analyte/NP mixtures.

1.6 Thesis objectives

Studies exist on the interaction of organodithiols with Au and Ag films as well as on NPs as has been discussed in Chapter 1 of this work. However, compared to planar films, studies on NPs have been somewhat limited. Of particular interest in this work is para-aryl dithiols (PADTs, HS-$(C_6H_4)_n$-SH, n =1, 2, and 3) which have found tremendous applications in several areas including molecular electronics, SERS, and quantum electron tunneling between two AuNPs and AgNPs. The PADTs are generally believed to act as single molecule dithiolate spacers in the majority of these applications without detailed structural studies of these molecules on the plasmonic NPs.

This dissertation is composed of three chapters. Chapter 1 provides an overview of the dissertation including the current state-of-knowledge of the subjects related to the dissertation. Chapter 2 of this dissertation is focused on the interaction of PADTs with AuNPs and AgNPs in an effort to have detailed understanding about their structure on these plasmonic NPs. As part of our continuing effort, the interactions, structures, and conformations of α,ω-alkanedithiols (ADTs), which have also been utilized in a number of areas were also studied. Chapter 3 of this work discusses the structures and orientations of ADTs on AuNPs and AgNPs in water. The insights provided in these studies have broad significance in NP research because of the increasing importance of these classes of organothiols in molecular electronics and SERS applications.

CHAPTER II

CAN PARA-ARYL-DITHIOLS CROSS-LINK TWO PLASMONIC NOBLE NANOPARTICLES AS MONOLAYER DITHIOLATE SPACERS?

(Published in *J. Phys. Chem. C* **2015**, 119, 6626-6633)

2.1 Abstract

Para-aryl-dithiols (PADTs, HS-$(C_6H_4)_n$-SH, n = 1, 2 and 3) have been used extensively in molecular electronics, surface-enhanced Raman spectroscopy (SERS), and quantum electron tunneling between two gold or silver nanoparticles (AuNPs and AgNPs). One popular belief is that these dithiols cross-link noble metal nanoparticles (NPs) as monolayer dithiolate spacers. Reported herein is our finding that PADTs predominantly exist as monothiolate forms on AuNPs and AgNPs. No PADT-induced NP cross-linking was observed regardless of the NP/PADT concentration ratios. Moreover, only one PADT thiol can be deprotonated, even when PADTs are treated with concentrated NaOH or $AgNO_3$ solutions. In contrast, 1,4-benzenedimethanethiol (HS-CH_2-(C_6H_4)-CH_2-SH) and the alkyl dithiol 1,2-ethanedithiol (EDT) can be completely deprotonated forming dithiolates on AuNPs and AgNPs, and in excess NaOH and $AgNO_3$ solutions.

2.2 Introduction

Para-aryl-dithiols (PADT) including 1,4- benzenedithiol (BDT), biphenyl-4,4'-dithiol (BPDT, HS-(C_6H_4)$_2$-SH), and *p*-terphenyl-4,4"-dithiol (TPDT, HS-(C_6H_4)$_3$-SH) have been used extensively in molecular electronics,[35, 80-83] SERS,[84-88] and in studying quantum electron tunneling between plasmonic resonators.[89] One popular belief is that the PADTs form dithiolates on plasmonic gold and silver nanoparticles (AuNPs and AgNPs) and cross-link nanoparticles (NPs) as single-molecular spacers.[35, 81, 82, 85, 87, 89, 90] However, direct experimental evidence for BPDT and TPDT are, to our knowledge, totally lacking. In the case of BDT, one key supporting evidence is that the characteristic S-H stretch Raman peak in ~2600 cm^{-1} region and C-H stretch in ~3100 cm^{-1} in the intact BDT becomes "invisible" when BDT is adsorbed on AuNPs and AgNPs or reacted with NaOH.[55, 90, 91] Since the C-H bonds should remain chemically intact in BDT reacted with NaOH or adsorbed onto NPs, the most reasonable explanation for the apparent disappearance of BDT C-H stretch feature is its low Raman activity in treated BDT. This raises a possibility that the apparent absence of the S-H stretch peak could also be due to low S-H Raman activity in these samples, but not to the BDT dithiolation. Indeed, our experimental investigation and computational simulation that will be shown later in this chapter indicate that the S-H and C-H Raman activities in PADT monothiolates are drastically lower than that in their respective intact PADTs. Consequently, the Raman and surface enhanced Raman spectroscopic (SERS) spectra of PADT monothiolates can be easily misinterpreted as their respective dithiolate counterparts, if one simply relies on the detectability of the S-H feature to deduce the degree of PADT thiolation.

Besides the three PADTs (BDT, BPDT, and TPDT), 1,4-benzenedimethanethiol (BDMT) and 1,2 ethanedithiol (EDT) were included as model molecules in this work. The molecular structures of the model dithiols used in this study are shown in Figure 2.1 below. All the model dithiols share the same general structure of HS-R-SH in which the two thiol groups are located at the distal end, but differ in the aromaticity and molecular size in their junction R groups (Figure 2.1). Therefore, this set of model molecules enables us to probe the effect of aromaticity as well as the size of the junction R on the chemical reactivity of the thiol groups. For the sake of simplicity, the notation of A/B was used to represent a two-component mixture solution of NP and dithiol.

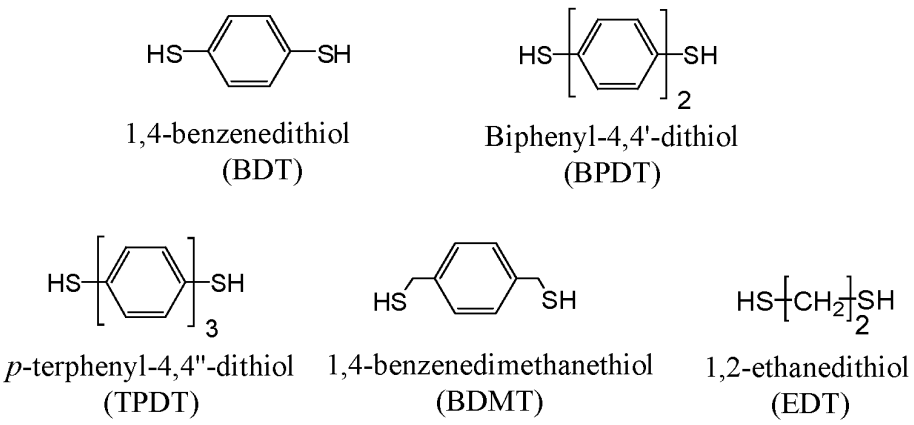

Figure 2.1 Molecular structures of the model molecules used in this study.

2.3 Experimental section

2.3.1 Materials and equipment

All chemicals were purchased from Sigma-Aldrich. The purities of the dithiols are BDT (97%), BPDT (95%), TPDT (96%), BDMT (98%), and EDT (≥ 98%). Water (18.2 MΩ cm) was used throughout the experiments. The RamChip slide used for the SERS

spectral acquisition was obtained from Z&S Tech LLC. It is important to note that the RamChip is a normal Raman substrate that is both fluorescence and Raman-background free.[92, 93] The normal Raman and SERS spectra were obtained with a Horiba LabRam HR800 confocal Raman microscope system and a 633 nm He-Ne Raman excitation laser. UV−visible measurements were taken using an Olis HP 8452 diode array spectrophotometer. TEM analysis was performed on a Joel 2100 instrument. Centrifugation was performed using a bench top Eppendorf centrifuge (model 5424).

2.3.2 Synthesis of AuNPs

AuNPs were prepared using the citrate reduction method.[94] Briefly, 0.042 g of gold(III) chloride•trihydrate was added to 150 mL of water (18.2 MΩ cm). The solution was brought to a boil, and then 3 mL of 1% sodium citrate dihydrate was added. The solution was kept boiling for approximately 1 h before cooling to room temperature. The surface plasmonic peak absorbance of the as-synthesized AuNPs is at 520 nm. A TEM image shows the particle size of in-house synthesized AuNPs is 13 ± 1.3 nm in diameter (Figure 2.2)

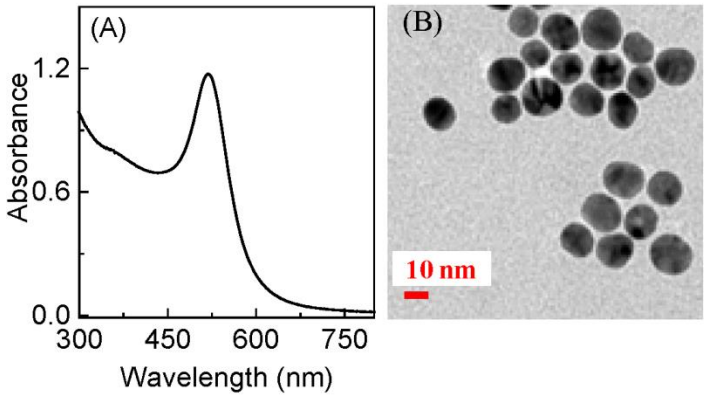

Figure 2.2 UV-vis spectrum and TEM image of the in-house synthesized AuNPs used in this study.

2.3.3 Synthesis of AgNPs

The AgNPs have also been synthesized in-house using the Lee-Misel method.[18] Briefly, 0.028 g of silver nitrate was added to 150 mL of Nanopure water, and the solution was brought to a boil. 3 mL of 1% sodium citrate dihydrate was then added. The solution was kept boiling for another ~1 h before cooling to room temperature. The surface plasmonic peak absorbance of the synthesized AgNPs is at 407 nm. The average particle size of the as-synthesized AgNP is 50 ± 9 nm in diameter, determined by TEM imaging (Figure 2.3).

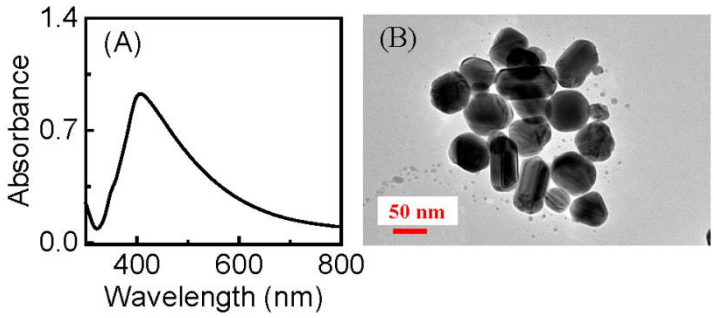

Figure 2.3 UV-vis spectrum and TEM image of the in-house synthesized AgNPs used in this study.

2.3.4 PADT, BDMT, and EDT binding with AuNPs and AgNPs

The time-dependent UV-vis measurements were taken using AuNP/dithiol or AgNP/dithiol mixtures in which the nominal concentration of the dithiol is 33 μM. The samples were prepared by mixing 1 mL of the synthesized AuNPs or 1 mL of two times diluted AgNPs with equal volume of water and 1 mL of dithiols. The nominal dithiol concentrations in the samples used for the dithiol concentration dependence study are 5 μM, 10 μM, 25 μM, and 50 μM. The dithiol solutions were prepared from stock BDT (1 mM in ethanol), BDMT (1 mM in ethanol), BPDT (2 mM in 50:50 chloroform/ethanol mixture), TPDT (400 μM in THF), and EDT (1 mM in ethanol) by further dilution with water. The nominal concentration of AuNPs in the sample mixtures is ~ 4.3 nM. The concentration of the AuNPs was calculated using the extinction coefficient of 2.7×10^8 M^{-1} for 13 nm particle diameter at 520 nm and assuming the AuNPs are spherical and monodispersed.[95] Time-resolved measurements were also performed for BDMT/AuNP and EDT/AuNP in which the nominal concentration of dithiol is 33 μM. Briefly, 1 mL of AuNPs was mixed with an equal volume of water followed by the addition of 1 mL of

BDMT or EDT. The mixture was stirred continuously during the time- resolved measurement. The time-interval between consecutive spectral acquisitions is 3 seconds.

2.3.5 Transmission Electron Microscopy (TEM)

TEM images for the dithiol-treated AuNP and AgNP samples were acquired for the washed precipitates of the mixtures after 4 d of sample incubation. Possible free PADTs, BDMT, and EDT in the sample mixtures were removed before TEM measurements. Since the BDMT and EDT induced spontaneous AuNP aggregation and settlement, the free dithiols in these mixtures was removed by simply washing the precipitates three times with Nanopure water. On the other hand, AuNPs in the PADT mixtures were stable (no aggregation). The removal of free PADTs in these mixtures was conducted by centrifugation followed by washing with copious amount of water. TEM images were taken with Cu grids covered with a Formvar carbon film at an accelerating voltage of 200 kV. The nominal concentration of PADTs, BDMT, and EDT in the samples used for TEM imaging is 33 μM.

2.3.6 Theoretical calculation of Raman spectra of PADTs and BDMT

All the quantum calculations were performed using the Gaussian 09 suite. The ground state structures of the PADTs or BDMT were optimized using density functional theory (DFT) method with BP86 functional at the level of 6-311++G (d, p) basis set. Frequency analysis was carried out and no imaginary frequencies were found, ensuring that all of the structures were minima. The Raman spectra were calculated based on these optimized structures using the same functional and basis set as geometry optimization. The calculated wavenumbers in Raman spectra were not scaled by any factor.

2.3.7 Normal Raman and SERS measurements

All the normal Raman and SERS spectra were taken with an Olympus 10× objective (NA = 0.25), and spectrograph grating of 300 grooves/mm. The laser intensities before entering the sample for normal Raman spectra and SERS spectra were 13 mW and 1.3 mW respectively. The spectral integration time varied from 5 s to 500 s. The Raman shift was calibrated with a neon lamp, and the Raman shift accuracy was ~0.5 cm^{-1}. The normal Raman spectra of the PADTs and BDMT were acquired using the solid powder samples, while that for EDT was obtained with neat EDT liquid. When it was needed, 1% KCl was used as the aggregation reagent to induce AuNP or AgNP aggregation before the SERS acquisitions. The concentrations of dithiols in the analyte concentration dependence SERS samples are 5 μM, 10 μM, 25 μM, and 50 μM. Normal Raman spectra of PADTs or BDMT in basic pH were obtained for supernatant of a saturated BDT or BDMT solution in 1 M NaOH after centrifugation at 15000 rpm for 10 min, or for molten state reaction products of PADTs with solid NaOH.

2.3.8 Molten-state PADT reaction with solid NaOH

Small amounts (~10 mg) of the PADTs were mixed with excess solid NaOH in a round bottom flask connected to a nitrogen flow source. The mixture of PADTs/NaOH was heated on a hot plate set to a temperature of ~350 ^{o} C under constant nitrogen flow for ~4 h. The resulting molten state reaction products of the PADTs were allowed to cool at room temperature for ~6 h under constant nitrogen flow. The normal Raman spectra were then obtained for the molten state reaction products taken from the bottom of the flask.

2.3.9 PADT, BDMT, and EDT reactions with $AgNO_3$

Dithiol reaction with $AgNO_3$ were conducted with stoichiometric ratio of dithiol:Ag of 1:1 and 1:300 respectively. The 1:1 molar ratio PADT: $AgNO_3$complexes were prepared by mixing BDT (1 mM in absolute ethanol), BPDT (1 mM in chloroform/ethanol mixture) or supernatant of saturated solution of TPDT (in THF) with an equal volume of 1 mM $AgNO_3$ in water. The mixtures were allowed to sit at room temperature overnight under constant shaking. Solvent was then removed by rotary evaporation when necessary to promote the Ag-thiolate precipitation, and the insoluble complexes were washed with copious amount of water. Similarly, the 1:300 molar ratio complexes were prepared by reacting appropriate volumes of the dithiol solutions with 1 M $AgNO_3$ solution. All the Ag-thiolate complexes were washed with water and dried at room temperature before Raman measurements.

2.4 Results and Discussions

2.4.1 PADT, BDMT, and EDT binding to AuNPs

PADTs differ drastically from BDMT and EDT in their binding with AuNPs (Figure 2.4). The possibility that PADTs cross-link AuNPs was excluded on the basis of UV-vis and SERS measurements of the PADT-treated AuNPs. No significant PADT-induced AuNP aggregations were observed regardless of the PADT/AuNP concentration ratios in which the amount of PADT changes from below monolayer packing to PADT in large excess (Figure 2.4, and Figure 2.5 and Figure 2.6). The relatively small red-shift of the AuNP LSPR peak in the PADT treated AuNPs in comparison to that of AuNP control is due to ligand adsorption that changes the dielectric constant of the medium immediately surrounding the AuNPs.[96-98]

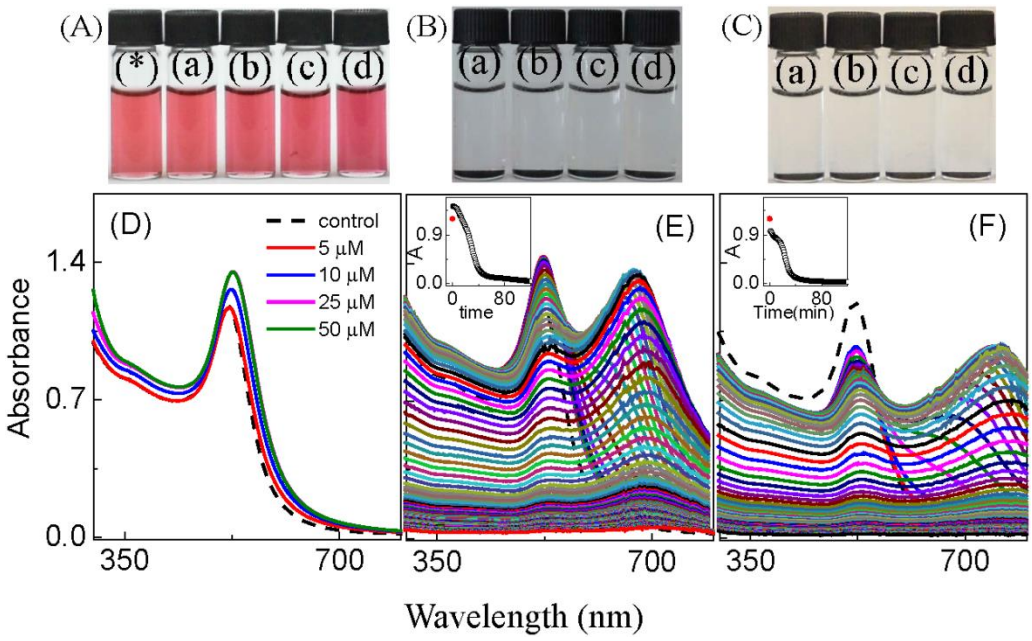

Figure 2.4 Photographs of the AuNPs mixed with (A) BDT, (B) BDMT, and (C) EDT of different concentrations after overnight incubation. (D) UV-vis spectra of the AuNP samples shown in (A). (E) and (F) are time-resolved UV-vis spectra of the BDMT/AuNP and EDT/AuNP mixtures respectively.

Note: The concentrations of model dithiols in vial (a)-(d) are 5 μM, 10 μM, 25 μM and 50 μM respectively. The vial labeled * is the AuNP control. The samples were prepared by mixing 1 mL of as-synthesized AuNPs with equal volume of water and dithiol respectively. The nominal AuNP concentration in the samples is ~4.3 nM. The dithiol concentration in the samples for time-resolved measurements is 33 μM. Inset in (E) and (F) is the plot of the absorbance of the AuNP LSPR at 520 nm as a function of time. The red dot in the time course is the peak UV-vis intensity of the AuNP control.

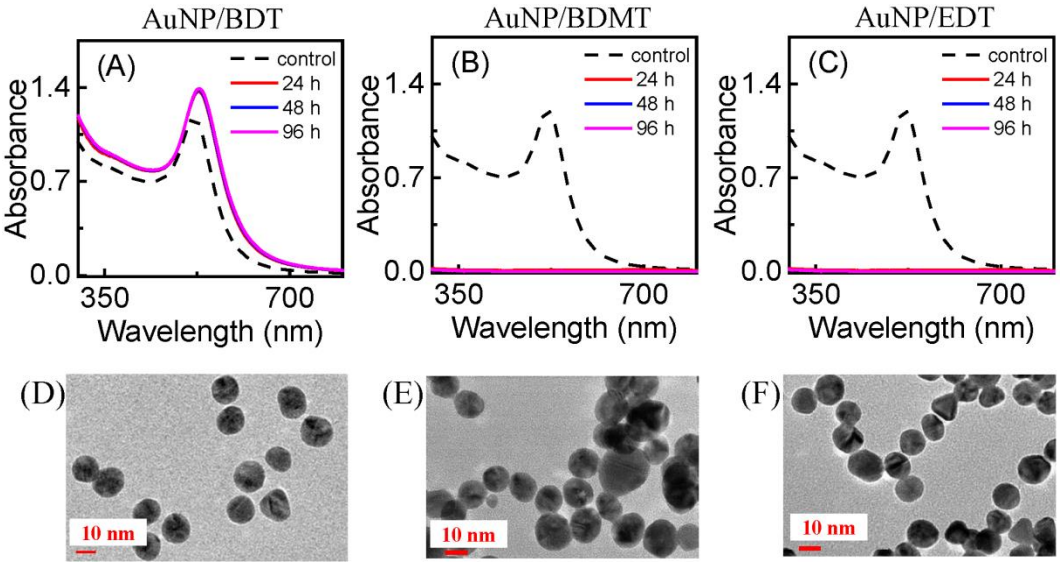

Figure 2.5 Time dependent UV-vis spectrum for AuNPs mixed with (A) BDT, (B) BDMT and (C) EDT. (D-F) TEM images of AuNP/BDT, AuNP/BDMT, and AuNP/EDT samples respectively.

Note: The concentration of dithiols in the samples used for the time dependent and TEM measurements is 33 μM. TEM images were taken for samples after 4 days of sample incubation.

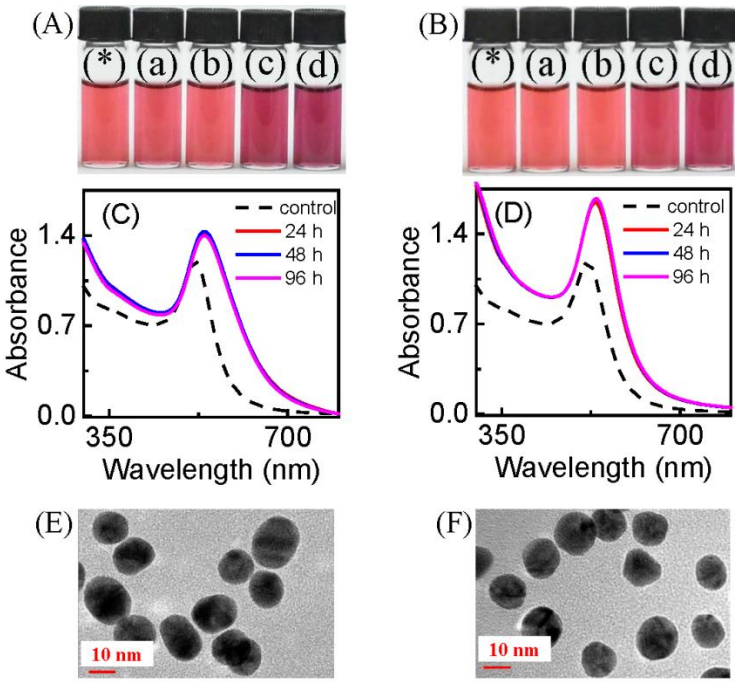

Figure 2.6 Photographs of the AuNPs mixed with (A) BPDT and (B) TPDT of different concentrations after overnight incubation. (C) and (D) are time dependent UV-vis spectra of the AuNP/BPDT and AuNP/TPDT samples respectively. (E) and (F) are TEM images of AuNP/BPDT and AuNP/TPDT samples respectively.

Note: The concentrations of model dithiols in vial (a)-(d) are 5 μM, 10 μM, 25 μM and 50 μM respectively. The vial labeled * is the AuNP control. The samples were prepared by mixing 1 mL of as-synthesized AuNPs with equal volume of the dithiol solutions and water. The dithiol concentration in the TEM and time dependent samples is 33 μM. TEM images were obtained after 4 days of sample incubation.

In stark contrast to the experimental data obtained with PADTs, BDMT and EDT binding with AuNPs induces immediate AuNP aggregation, and eventual AuNP settlement to the bottom of the glass vial (Figures 2.4(B) and 2.4(C)). The AuNP settlement is deduced from the total absence of the AuNP LSPR peak in the time-resolved UV-vis spectra taken with the BDMT/AuNP and EDT/AuNP one hour after the sample preparation (Figures 2.4(E) and 2.4(F)). Complete AuNP aggregation and settlement were observed in all the tested BDMT/AuNP and EDT/AuNPs mixtures. It

should be noted that the concentration ratios in the series of PADT/AuNP samples are the same as that in the corresponding BDMT/AuNP and EDT/AuNP samples. This result strongly suggests that the aromaticity of junction R group in the organodithiol of HS-R-SH has drastic effect on the dithiol reaction with AuNPs.

Importantly, the PADT-containing AuNPs remained stable in water (no aggregation) for at least six months after sample preparation. Figure 2.7 below is the photograph taken for AuNP/PADT mixtures after 6 months of sample incubation.

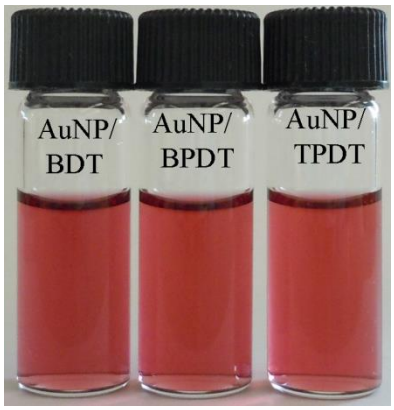

Figure 2.7 Photographs of AuNP/BDT, AuNP/BPDT, and AuNP/TPDT mixtures after incubation for ~ 6 months.

Note: The nominal concentration of dithiol in the samples is 25 μM. The mixtures remain stable even after ~6 months incubation at room temperature.

While the absence of AuNP aggregation can serve as an unequivocal evidence that PADT did not induce AuNP cross-linking, the fact that BDMT and EDT induced AuNP aggregation does not necessarily imply that AuNPs are cross-linked in which BDMT or EDT acts as a single-molecule dithiolate spacer. This is because both BDMT and EDT can adopt multiple possible structures and conformations on the AuNP surfaces. Many ligands such as adenine and methylbenzenethiol induce rapid AuNP aggregation

even though they are unable to induce AuNP cross-linking.[99, 100] Indeed, SERS measurements indicate that BDMT and EDT structure and conformation depends strongly on the dithiol concentration (Figures 2.8(B) and 2.8(E), and 2.8(C) and 2.8(F)). BDMT and EDT exist as dithiolate only when their concentrations are low. This is evidenced by the absence of detectable S-H feature in the ~2600 cm^{-1} region in the BDMT and EDT SERS spectra on AuNPs when the dithiol concentration is at ~10 μM or lower. In this case, the two sulfurs in BDMT and EDT are either both anchored to the same AuNP (Figures 2.9A and 2.9G) or each links to a different AuNP (Figures 2.9B and 2.9H). These two conformers may concurrently exist for sparsely packed BDMT and EDT on AuNP surfaces. Unfortunately, it is currently impossible to pinpoint which configuration is the dominant one.

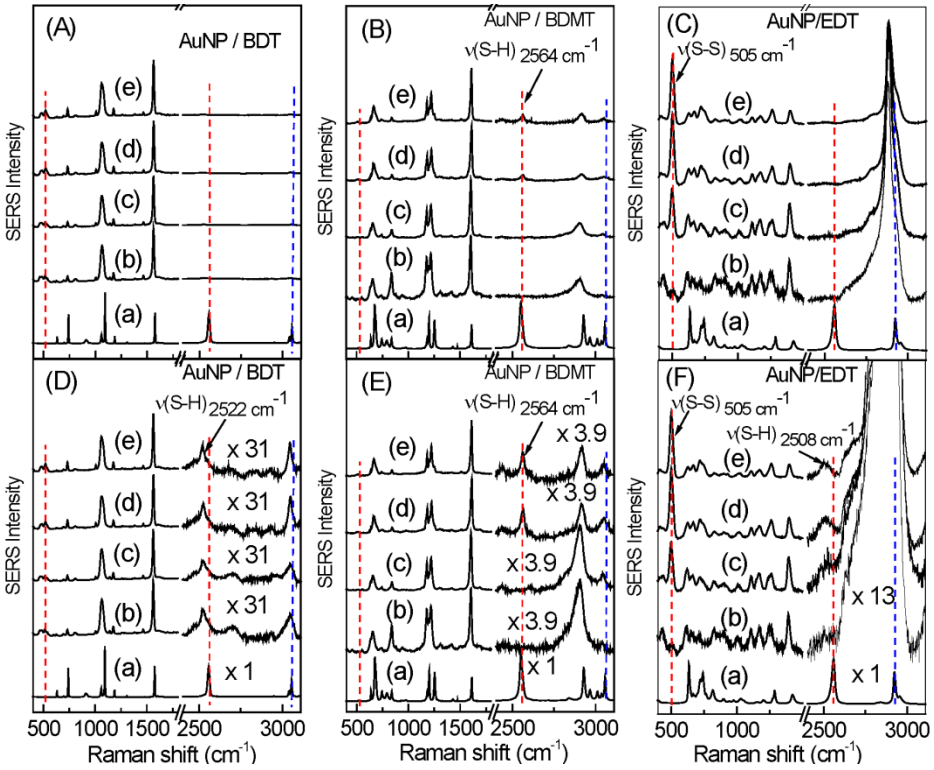

Figure 2.8 SERS comparison of (*Left*) BDT, (*Middle*) BDMT, and (*Right*) EDT interactions with AuNPs.

Note: The SERS samples (b)-(e) have the identical composition as that shown in Figure 2.4 (a)-(d). Spectrum (a) is the normal Raman spectrum of BDT, BDMT and EDT. KCl (1%) was used as the aggregation agent for the SERS measurements of the BDT samples. The dotted lines from the left to right indicate expected peak positions for S-S, S-H, and C-H features. Spectra in plots (D-F) are the same as their corresponding ones in (A-C), but the spectral features in (D-F) were magnified in the region from 2400 cm^{-1} to 3200 cm^{-1} by the specified factors. No significant S-S formation is observed in the ~510 cm^{-1} region for both BDT and BDMT.

BDMT is primarily in an upright monothiolate form on AuNPs when it is densely packed on AuNPs (Figure 2.9C). This conclusion is drawn from the presence of a relatively strong S-H peak in the ~2600 cm^{-1} region and the absence of a S-S stretch feature in the SERS spectra obtained with samples of high BDMT/AuNP concentration ratios (Figure 2.8 (E)). If there is significant AuNP cross-linking by single-molecule BDMT dithiolates (Figure 2.9B), those dithiolate molecules should be located in the most

SERS active NP junctions and dominate the BDMT SERS spectra. No S-H peak would be observable in this case. Similarly, if there is significant disulfide-formation between BDMTs directly anchored on the same AuNPs (Figure 2.9D) or between surface adsorbed BDMT and BDMT free in solution (Figure 2.9E), or between BDMTs adsorbed on different AuNPs (Figure 2.9F), one should observe a relatively strong S-S peak in the ~510 cm^{-1} region as seen in SERS spectra obtained with densely packed EDT on AuNPs. The latter indicates that EDT molecules are substantially disulfide-linked on the AuNPs when excess EDT is added onto AuNPs (Figure 2.8(C) and 2.8(F)). Similar EDT disulfide-linkage on AuNPs were reported before.[54]

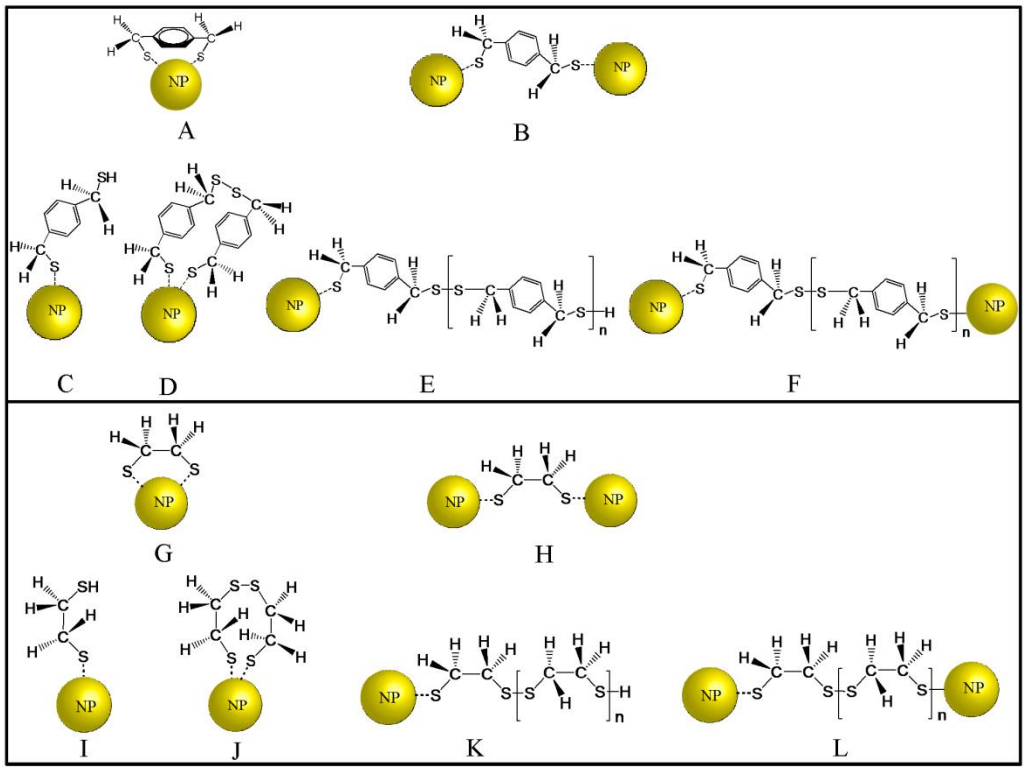

Figure 2.9 Possible (*Top*) BDMT and (*bottom*) EDT structures on AuNPs.

Note: (A) and (B), (G) and (H) are when BDMT and EDT are sparsely packed respectively. (C-F) and (I-L) are when BDMT and EDT are densely packed respectively onto AuNPs.

Such linkage can occur between two EDT molecules that are both directly anchored on the same AuNPs (Figure 2.9J) or between surface adsorbed EDT and EDT free in solution (Figure 2.9K), or between EDTs adsorbed on different AuNPs (Figure 2.9L).

The SERS spectra of BDT/AuNP are remarkably different from those obtained with BDMT/AuNPs and EDT/AuNPs (Figure 2.8), which is consistent with the sharp difference between the UV-vis spectra of BDT/AuNP samples and their BDMT/AuNPs and EDT/AuNPs counterparts (Figure 2.4). The BDT SERS spectra on AuNPs are entirely independent of the BDT/AuNP concentration ratio (besides the spectral signal-to-

noise ratio). There is a relatively strong S-H stretch peak (relative to the C-H stretch feaure) in the BDT SERS spectra and no detectable S-S feature regardless of the BDT concentration. This result shows that BDT predominaintly adopted a monothiolate form on the AuNPs in all the samples (Figure 2.8(D)). This conclusion is in sharp contrast to the popular belief that BDT binds as dithiolate onto AuNPs and gold electrode.[35, 81, 82, 89, 90]

Indeed, the relatively strong S-H and C-H stretch peaks in the normal Raman of intact BDT become essentially "invisible" in the SERS spectra obtained with BDT adsorbed onto AuNPs (Figure 2.8 (A)). Similar BDT SERS spectra have been reported before.[55, 90, 91] The poor detectability of the S-H was viewed as evidence of BDT dithiolation on plasmonic NPs, while the reason for the absence of the C-H peak has not been investigated. However, the magnified spectra clearly showed the presence of both S-H and C-H peaks in the SERS spectra obtained with BDT on AuNPs (Figure 2.8 (D)). Fruitfully, the experimental SERS spectrum is in excellent agreement with computationally-simulated BDT monothiolate spectrum and the experimental normal Raman spectrum of the silver BDT-monothiolate salt prepared by mixing BDT with $AgNO_3$ with 1:1 molar ratio (Figure 2.10).

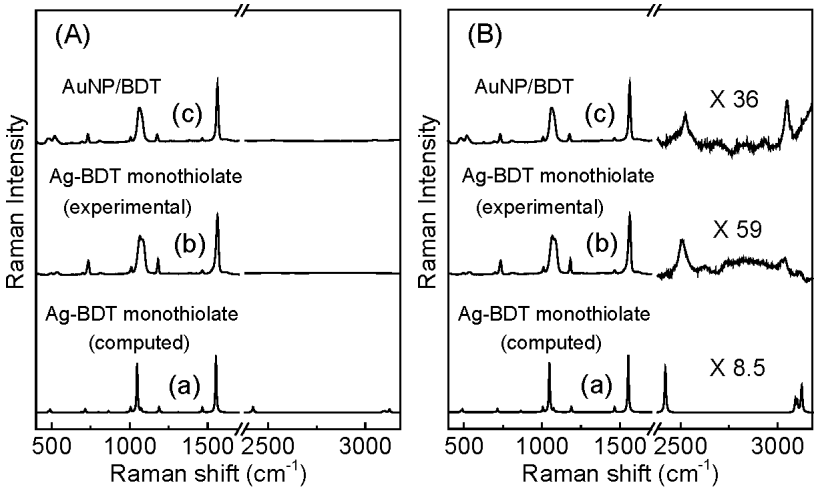

Figure 2.10 (A) Computed Raman spectra (a) and experimental Raman spectra (b) of silver-BDT monothiolate. Spectrum (c) is the SERS spectrum of BDT on AuNPs.

Note: Plot (B) is the same as (A), but the spectral feature from 2400 cm^{-1} to 3200 cm^{-1} was magnified by factors specified in each spectrum. The molar ratio of $AgNO_3$: BDT in spectrum (b) is 1:1. The nominal concentration of BDT in the SERS sample is 33 μM. BDT on AuNPs is primarily in the monothiolate form.

This allows us to conclude that BDT on AuNPs is primarily in a monothiolate form. It also enables us to conduct peak assignments with high confidence. The peak assignment for the PADTs is shown in Figure 2.11 below. Table 2.1 also shows the different vibrational modes (C-H stretch, C-H bending, C-C stretch and S-H stretch) together with their peak assignments.

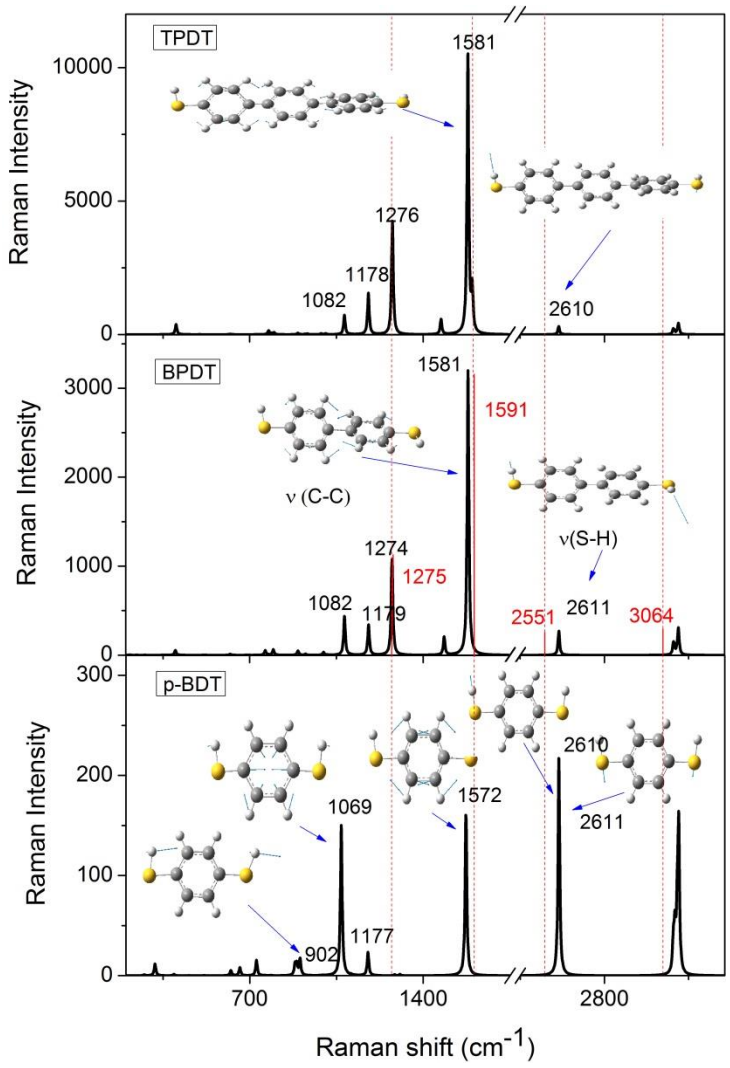

Figure 2.11 The computed normal Raman spectrum of BDT, BPDT and TPDT.

Note: The insets show the normal mode vectors. For BPDT, peak at 1581 cm^{-1} is assigned for C-C stretching mode, and 2611 cm^{-1} is assigned for S-H stretching mode. The vertical red lines represent the peak positions in experimental normal Raman spectra obtained with the intact PADT solids.

Table 2.1 Vibrational modes and peak assignments for normal Raman spectra of PADTs

Vibrational modes and peak assignments		
BDT	BPDT	TPDT
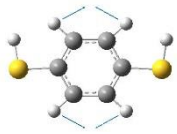 C-H bending ($1177\ cm^{-1}$)	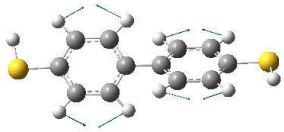 C-H bending ($1179\ cm^{-1}$)	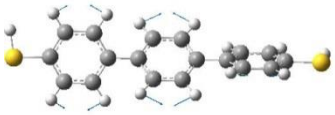 C-H bending ($1178\ cm^{-1}$)
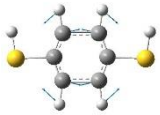 C-C stretching ($1572\ cm^{-1}$)	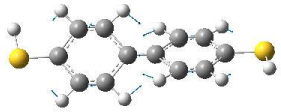 C-C stretching ($1581 cm^{-1}$)	 C-C stretching ($1581 cm^{-1}$)
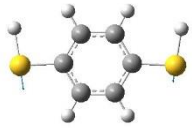 S-H stretching ($2611\ cm^{-1}$)	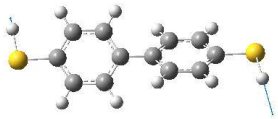 S-H stretching ($2611\ cm^{-1}$)	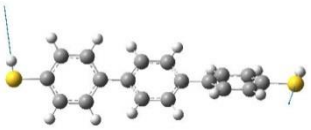 S-H stretching ($2610\ cm^{-1}$)
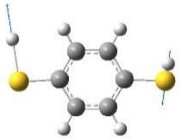 S-H stretching ($2610\ cm^{-1}$)	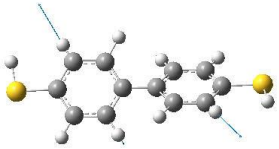 C-H stretching ($3086\ cm^{-1}$)	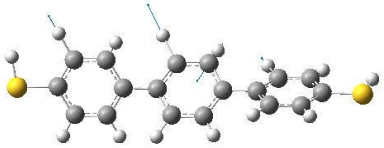 C-H stretching ($3085\ cm^{-1}$)
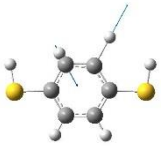 C-H stretching ($3087\ cm^{-1}$)	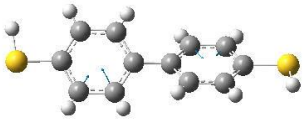 C-H stretching ($3108\ cm^{-1}$)	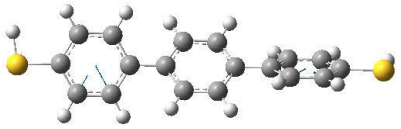 C-H stretching ($3109\ cm^{-1}$)
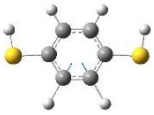 C-H stretching ($3109\ cm^{-1}$)		

The relative Raman activities of both C-H and S-H stretches for BPDT and TPDT are drastically smaller than respective counterparts for BDT. This conclusion is drawn by using the C-C stretch peak at ~1580 cm^{-1} as the internal reference. The experimental C-H and C-C Raman intensity ratio decreases from 0.52 for intact BDT to 0.06 and 0.02 for intact BPDT and TPDT respectively (Figure 2.12(A) and 2.12(C)). This is very surprising given the fact that the number ratios of C-C versus C-H bonds are identical among these PADT molecules. The experimental S-H and C-C Raman activity ratio, obtained by dividing the S-H/C-C Raman intensity ratio by their chemical bond number ratio decreases from 1.92 for intact BDT to 0.53 and 0.24 for intact BPDT and TPDT respectively (Figure 2.12(A) and 2.12(C)). Monothiolation of the BPDT and TPDT further reduces the C-H and S-H Raman activities. DFT calculated Raman spectra also are in excellent agreement with the experimental counterparts (Figure 2.12). The low S-H and C-H Raman activity in BPDT and TPDT make it exceedingly difficult for reliable spectral acquisition and interpretation.

Like BDT, BPDT and TPDT exist primarily in their monothiolate forms on AuNPs. This conclusion is drawn from the following experimental observations. First, there is a small, but detectable S-H peak in the BPDT and TPDT SERS spectra magnified in the spectral region from 2400 cm^{-1} to 3200 cm^{-1}. Second, the BPDT and TPDT SERS spectra are very similar to the Raman spectra of their respective monothiolate salt prepared by mixing BPDT or TPDT with $AgNO_3$ with 1:1 mole ratio (Figure 2.12(D)). Third, the dispersion stability and SERS spectral characteristics of AuNPs functionalized with BPDT and TPDT are similar to that for BDT- functionalized AuNPs, but differ drastically from BDMT- and EDT-functionalized AuNPs. This result suggests that the

BPDT and TPDT structures on AuNPs should be very similar to that for BDT, but different from that for BDMT and EDT.

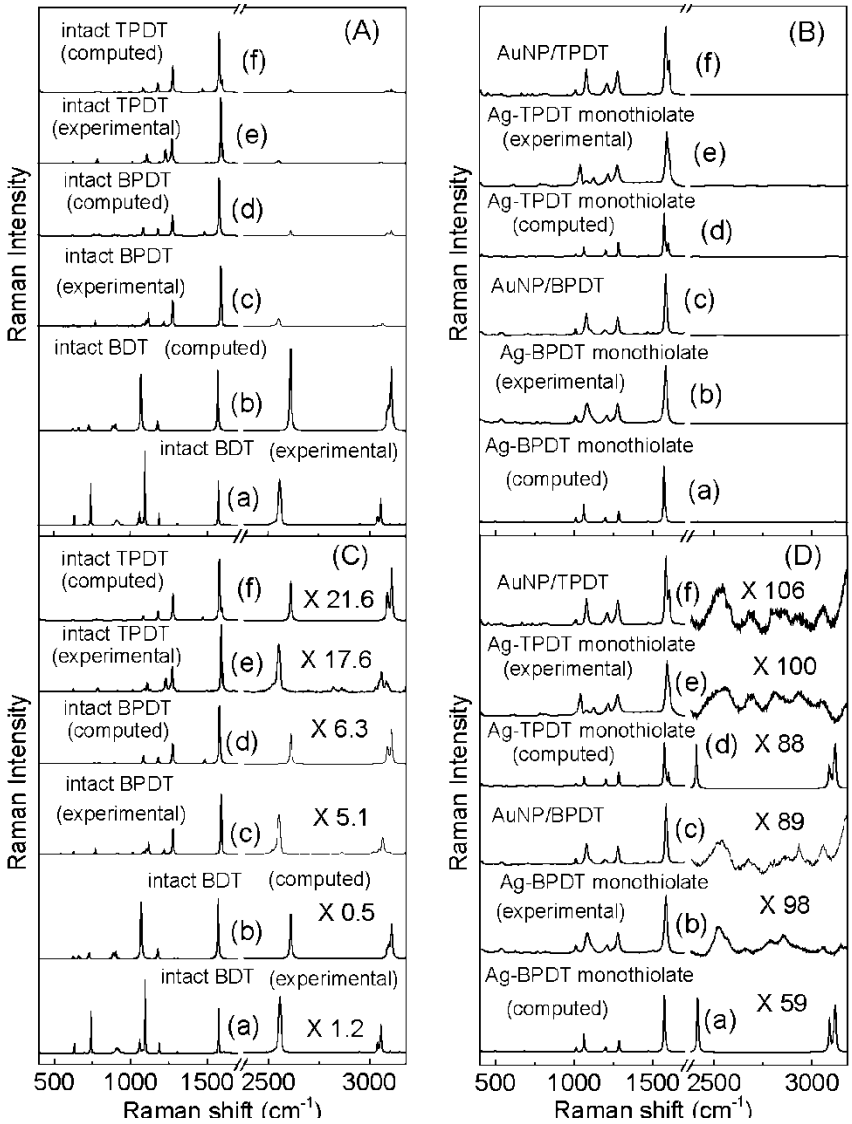

Figure 2.12 (*Left*) Experimental and computed Raman spectra of BDT, BPDT, and TPDT. (*Right*) Experimental and computed Raman spectra of the Ag-BPDT and Ag-TPDT monothiolate salts, and experimental SERS spectra of BPDT and TPDT on AuNPs.

Note: Spectra in plots (C) and (D) are the same as their corresponding ones in (A) and (B), but the spectra in (C) and (D) were magnified in the spectral region from 2400 cm^{-1} to 3200 cm^{-1} by factors specified in each spectrum.

This fact that BPDT and TPDT SERS spectra are independent of the ligand concentrations (Figure 2.13) is also consistent with the conclusion that BPDT and TPDT can only adopt a monothiolate form on AuNPs. Otherwise, no S-H peak should be observable when low concentration BPDT and TPDT were mixed with AuNPs in which the two thiols should be totally deprotonated as that for BDMT and EDT.

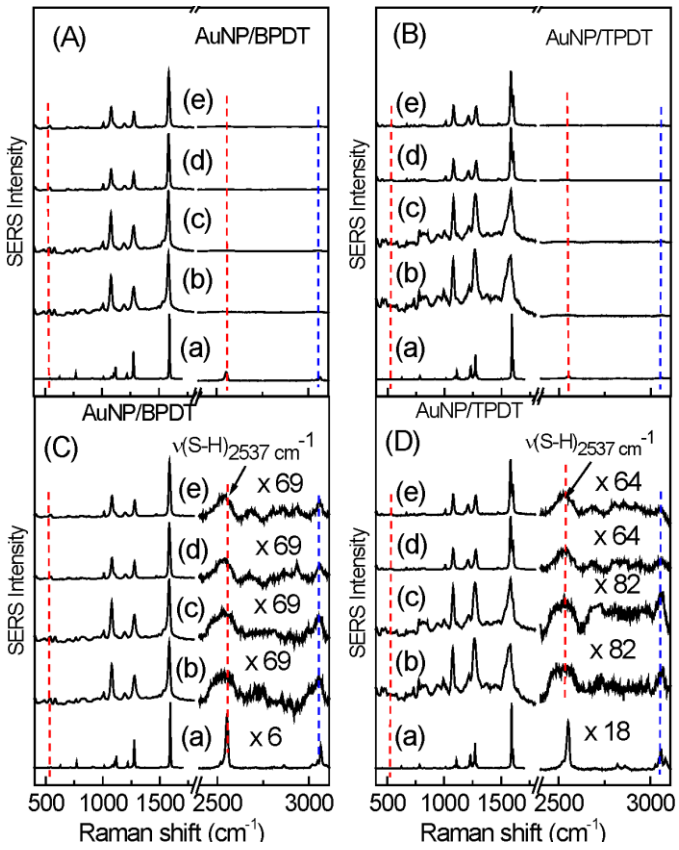

Figure 2.13 Analyte concentration dependence SERS spectra on AuNPs for (*Left*) BPDT, and (*Right*) TPDT.

Note: The SERS samples (b)-(e) have the identical composition as that shown in (a)-(d) of Figure 2.6 (A) and (B). Spectrum (a) is the normal Raman spectrum of BPDT and TPDT. KCl (1%) was used as the aggregation agent for the SERS measurements. The dotted lines from the left to right indicate expected peak positions for S-S, S-H, and C-H features. No significant S-S formation is observed in the ~520 cm^{-1} region for both BPDT and TPDT. Plots (C) and (D) are the same as (A) and (B) respectively, but the spectral feature from 2400 cm^{-1} to 3200 cm^{-1} were magnified by factors specified in each spectrum.

2.4.2 PADT, BDMT, and EDT binding with AgNPs

Possibilities of PADT, BDMT, and EDT inducing signficant AgNP cross-linking as single-molecular dithiolate spacers were excluded on the basis of the UV-vis and TEM study (Figure 2.14 and Figure 2.15) and SERS spectra (Figure 2.17 and Figure 2.18).

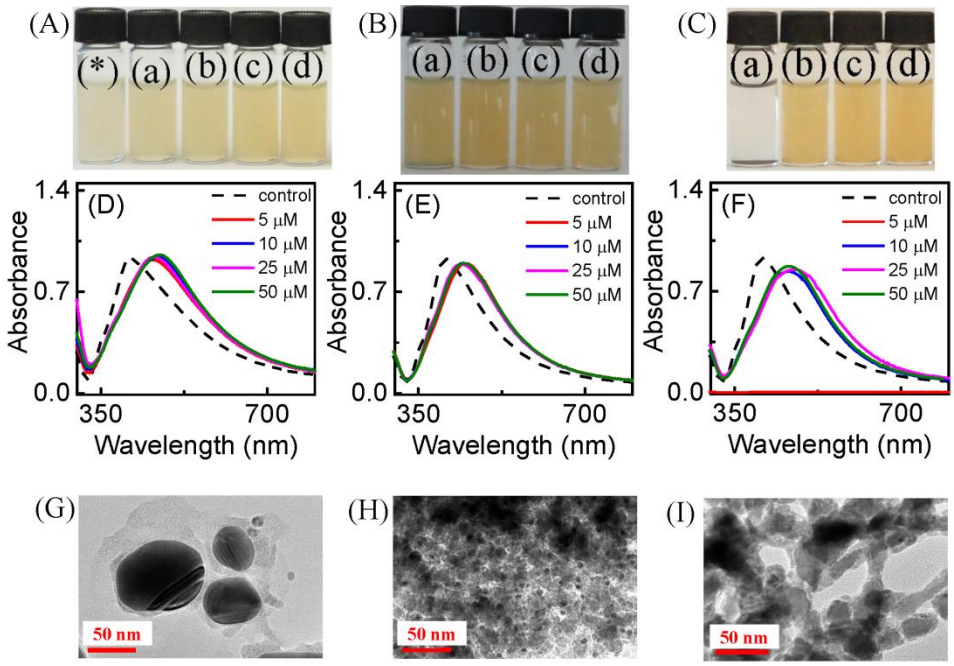

Figure 2.14 Photographs of the AgNPs mixed with (A) BDT, (B) BDMT and (C) EDT of different concentrations after overnight incubation. (D-F) UV-vis spectra of the AgNP samples shown in (A), (B), and (C) respectively. (G-I) are TEM images of the mixture obtained with AgNP mixed with BDT, BDMT and EDT respectively.

Note: The concentrations of model dithiols in vial (a)-(d) are 5 μM, 10 μM, 25 μM and 50 μM respectively. The vial labeled * is the AgNP control. The nominal concentration of dithiols in the TEM samples is 33 μM. TEM images were taken after 4 days of sample incubation. The scale bars in the TEM images are 50 nm.

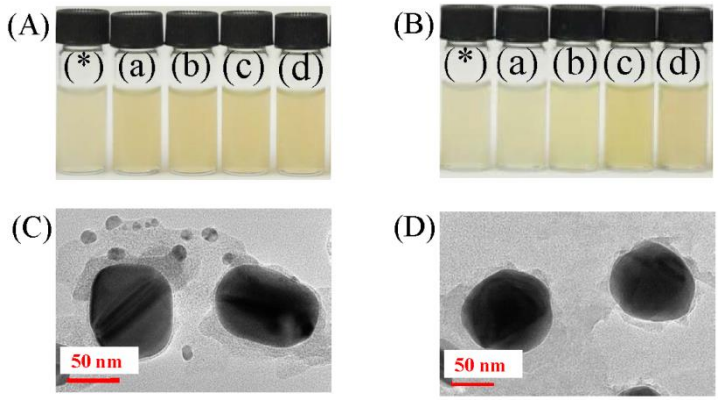

Figure 2.15 Photographs of the AgNPs mixed with (A) BPDT and (B) TPDT of different concentrations. (C) and (D) are TEM images of AgNP/BPDT and AgNP/TPDT samples respectively.

Note: The concentrations of model dithiols in vial (a)-(d) are 5 μM, 10 μM, 25 μM and 50 μM respectively. The vial labeled * is the AgNP control. The samples were prepared by mixing 1 mL of two-times diluted AgNPs with equal volume of water and dithiol. The dithiol concentration in the TEM samples is 33 μM. TEM images were obtained after 4 days of sample incubation.

These dithiol binding to AgNPs are remarkably different from their binding to AuNPs. First, the AgNPs mixed with these dithiols are highly stable (no aggregation) in the freshly prepared dithiol/AgNP mixtures. With the only exception of EDT at low concentration, no significant AgNP aggregations were oberved in one day after the sample preparation (Figure 2.14). However, precipitates appeared in all the samples after six months of the sample incubation under ambient conditions (Figure 2.16). This is in sharp contrast to their binding to AuNPs in which AuNPs in PADT containing solution are entirely stable, but BDMT and EDT induces immediate AuNP aggregation and settlement (Figure 2.4, 2.5, and 2.6).

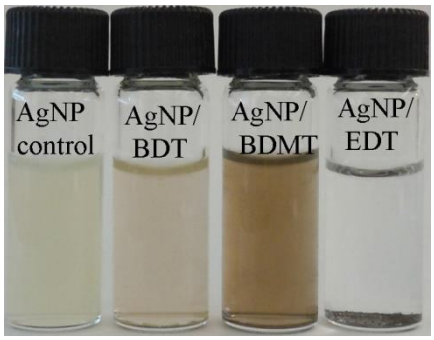

Figure 2.16 Photographs of BDT/AgNP, BDMT/AgNP, and EDT/AgNP mixtures after long term incubation (~ 6 months).

Note: The nominal concentration of dithiol in the samples is 25 μM.

TEM images obtained with the centrifuged precipitates of the four-day aged dithiol/AgNP samples showed that besides AgNPs, there are relatively large amount of insoluble amorphous material that coprecipitate with AgNPs (Figure 2.14 and Figure 2.15). Similar insoluble precipitates are presumably the Ag-PADT, Ag-BDMT, and Ag-EDT salts. It is noted that the AgNPs used in Figure 2.14 are the same for all the dithiols. Therefore, the more significant AgNP disintegration in BDMT/AgNP and EDT/AgNP samples than that in BDT/AgNP suggests that the two nonaromatic dithiols are more reactive than BDT with AgNPs (Figure 2.14).

The TEM images obtained with the AgNP samples are in stark contrast to that obtained with PADT-, BDMT-, and EDT-treated AuNPs in which no AuNP morphological changes were found (Figure 2.5 and Figure 2.6). These difference provides further supporting evidence of recent reports that organothiol bindings to AgNPs can be drastically different from that to AuNPs.[101-105] Mechanistic study revealed that the organothiol binding to AuNPs occurs by releasing the sulfur-bound hydrogen atoms as protons, thereby the organothiol is in thiolate form on AuNPs.[101] In contrast,

organothiol interacting with AgNPs proceeds by converting the surface silver oxide and surface silver atom into silver thiolate salt.[102] The formation of the silver thiolate salt layer on AgNPs exclude the possiblity for the dithiols to cross-link two AgNP as monolayer dithiolate linker.[87-89]

The SERS spectra of PADTs on AgNPs (Figures 2.17(A) and 2.17(D)) and Figure 2.18) are highly similar to that obtained with the PADTs on AuNPs. There is also a relatively intense S-H stretch peaks in comparision to the C-H stretch peak regardless of the PADT/AgNP concentration.

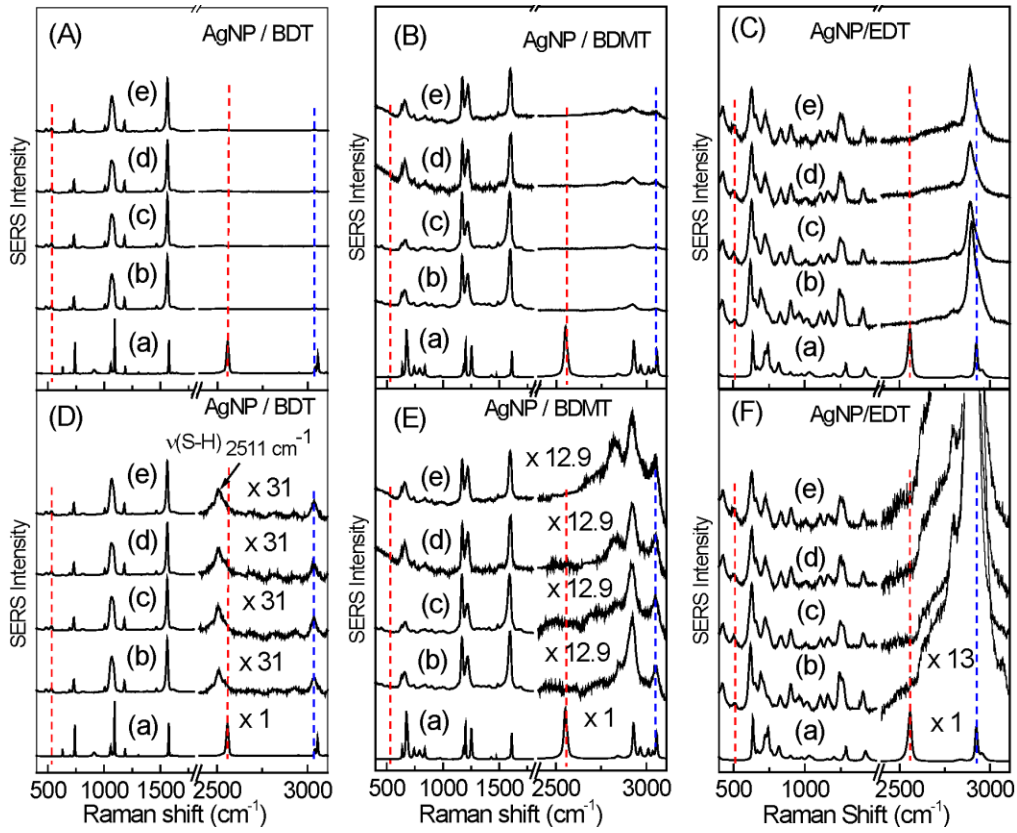

Figure 2.17 SERS comparison of (*Left*) BDT, (*Middle*) BDMT, and (*Right*) EDT interactions with AgNPs.

Note: The SERS samples (b)-(e) have the identical composition as that shown in Figure 2.14(a)-(d). Spectrum (a) in the plots is the normal Raman spectrum of BDT, BDMT, and EDT. KCl (1%) was used as the aggregation agent for the SERS measurements. The dotted lines from the left to right indicate expected peak positions for S-S, S-H, and C-H features. Spectra in plots (D-F) are the same as their corresponding ones in (A-C), but the spectral feature in (D-F) were magnified in the region from 2400 cm^{-1} to 3200 cm^{-1} by the specified factors. No significant S-S formation is observed in the ~510 cm^{-1} region for BDT, BDMT, and EDT.

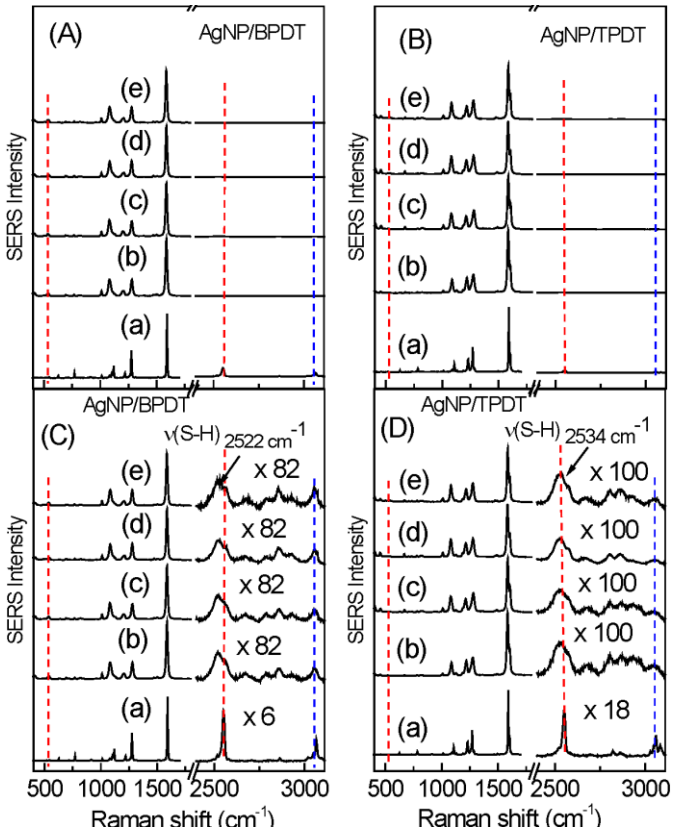

Figure 2.18 Analyte concentration dependence SERS spectra for (*Left*) BPDT, and (*Right*) TPDT on AgNPs.

Note: The SERS samples (b)-(e) have the identical composition as that shown in (a)-(d) of Figure 2.15. Spectrum (a) is the normal Raman spectrum of BPDT and TPDT. KCl (1%) was used as the aggregation agent for the SERS measurements. The dotted lines from the left to right indicate expected peak positions for S-S, S-H, and C-H features. No significant S-S formation is observed in the ~520 cm^{-1} region for both BPDT and TPDT. Plots (C) and (D) are the same as (A) and (B) respectively, but the spectral feature from 2400 cm^{-1} to 3200 cm^{-1} was magnified by factors specified in each spectrum.

This result indicates that the PADTs exist primarily in monthiolate form on AgNP. However, BDMT and EDT are predominantly in dithiolate form on AgNPs. No S-H or S-S features are observed in the SERS spectra of BDMT and EDT on AgNPs regardless of the BDMT/AgNP or EDT/AgNP concentration ratio investigated. These results indicate that the two thiols in both EDT and BDMT are both reactive to AgNPs or the silver ion derived from the AgNPs, but only one PADT thiol can react with AgNPs.

PADTs also differ significantly from BDMT and EDT in their reactions with $AgNO_3$ and NaOH. Only one PADT thiol is deprotonated even when PADT is treated with 300 times excess $AgNO_3$, with concentrated NaOH or solid NaOH (Figure 2.19). In contrast, complete thiol deprotonation is observed when BDMT and EDT are treated with excess NaOH and $AgNO_3$ (Figure 2.20).

The fact that only one PADT thiol can be deprotonated strongly suggest the chemical reactivity of the first and second PADT thiol are drastically different. In contrast, the chemical reactivity between the two thiols in BDMT and EDT are much more similar. These results indicate that the aromaticity of the junction R group is very critical in defining thiol reactivity difference in the organodithiols. When one PADT thiol is deprotonated, the negative charge on the sulfide group is delocalized through the aromatic benzyl ring(s) to the sulfur in the remaining thiol. This can increase the sulfur alkalinity in the second thiol group, making it difficult for the remaining PADT thiol to be deprotonated. In contrast, the two nonconducting methylene groups between the two thiols in BDMT and EDT prohibit effective charge transfer from sulfide to thiol. Therefore, deprotonation of one BDMT or EDT thiol has no significant effect on the reactivity of the second thiol. Consequently, the two BDMT thiols have similar chemical reactivities.

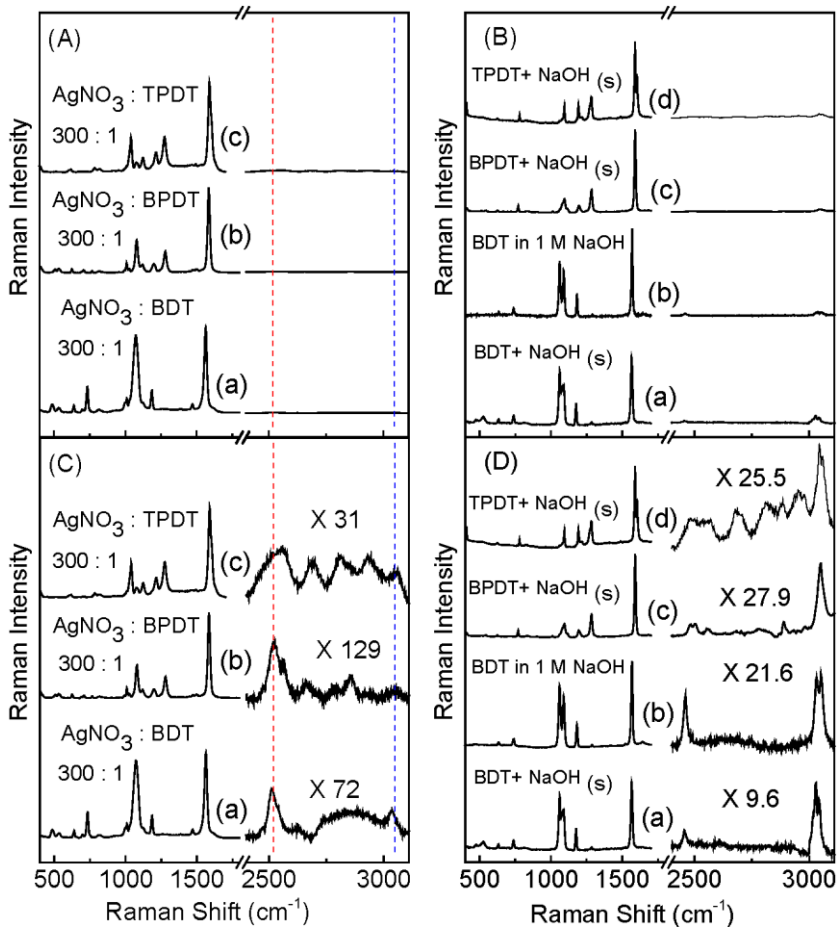

Figure 2.19 (A) Raman spectra of silver-PADT momothiolates where the mole ratio of silver: PADT is 300:1 for (a) BDT, (b) BPDT and (c) TPDT. (B) Raman spectra obtained with (a) molten BDT reacted with solid NaOH, (b) BDT in 1 M NaOH (c) BPDT, and (d) TPDT reaction products with excess NaOH.

Note: The molten state reactions were carried out as described in the experimental section of this chapter. (C) and (D) are the same spectra as in (A) and (B), but the spectral features from 2400 cm^{-1} to 3200 cm^{-1} were magnified by factors specified in each spectrum.

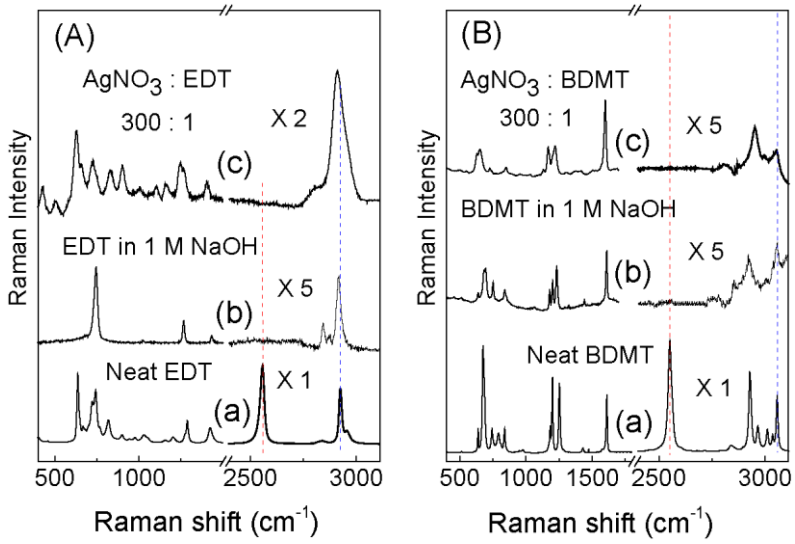

Figure 2.20 Raman spectra of (A) EDT and (B) BDMT in 1 M NaOH and in excess $AgNO_3$.

Note: spectra (b) was obtained in 1 M NaOH and spectra (c) is for silver-BDMT or silver-EDT complexes where the mole ratio of silver : dithiol is 300:1. Raman spectra of the dithiols were obtained with EDT (116 mM) in 1M NaOH or supernatant of a saturated solution of BDMT in 1 M NaOH.

2.5 Conclusion

In summary, PADT, BDMT, and EDT interactions with AgNPs and AuNPs were studied using combination of UV-vis, TEM, and SERS. No PADT-induced AuNP or AgNP cross-linking were observed under any of the investigated experimental conditions. The SERS measurements revealed that PADTs on AuNPs and AgNPs exist predominantly as monothiolates, but not dithiolates as believed in literature. Appreciable dithiolation of BDMT and EDT only appeared on AuNPs when the dithiol concentrations are low. Even under such conditions, the possiblibity for these dithiols to cross-link two AuNPs as single-molecular dithiolate spacers is likely low. This is because the two BDMT and EDT thiol groups are more likely attached to the same AuNP, instead of bridging two different AuNPs. The latter processs is likely kinetically less favorable than

the former because of the low AuNP concentration (~ nM) used in typical AuNP binding experiments. The findings and insights provided in this work should be important for a wide range of plasmonic NP studies where organodithiol and SERS measurements are commonly involved.

Notes: This work has been previously published: Gadogbe, M.; Chen, M.; Zhao, X.; Saebo, S.; Beard, D. J.; Zhang, D., Can Para-Aryl-Dithiols Cross-Link Two Plasmonic Noble Nanoparticles as Monolayer Dithiolate Spacers? *J. Phys. Chem. C* **2015**, 119, 6626-6633.

CHAPTER III

STRUCTURES AND CONFORMATIONS OF ALKANEDITHIOLS ON GOLD AND SILVER NANOPARTICLES IN WATER

(Published in *J. Phys. Chem. C* **2015,** *119*, 18414-18421)

3.1 Abstract

Organodithiols with two distal thiols have been used extensively in gold and silver nanoparticle (AuNP and AgNP) applications. However, understanding the structures and conformations of organodithiols on these nanoparticles (NPs) is challenging. Reported in this work is a combined surface enhanced Raman spectroscopy (SERS), transmission electron microscopy (TEM), inductively-coupled plasma mass-spectrometry (ICP-MS), and localized surface plasmonic resonance (LSPR) study of α,ω-alkanedithiol (ADT, (HS-$(CH_2)_n$-SH, n = 2, 4, and 6) interactions with AuNPs and AgNPs in water. These complementary techniques revealed a series of new insights that would not be possible using individual methods. A large-fraction of ADTs lies flat on AuNP surfaces. The upright ADTs are dimerized horizontally through disulfide-bond, or remain as monothiolates on the AuNP surfaces. Possibility of significant amount of vertically disulfide-linked organodithiol on the surface is excluded on the basis of ICP-MS and AuNP LSPR experiments. ADTs induced significant AgNP disintegrations in which ADTs are predominantly in dithiolate forms. This work highlights the extraordinary complexity of organodithiol interactions with plasmonic NPs. The insights

provided in this work will be important for enhancing fundamental understanding of the structure and properties of organodithiol-functionalized AgNPs and AuNPs.

3.2 Introduction

Organodithiols (HS-R-SH) with two distal thiol groups have been used as molecular linkers (spacers) in quantum plasmon coupling between nanoparticles (NPs),[106-108] molecular electronics,[34, 109-111] and SERS.[36, 112] While it is generally assumed that organodithiols exist as dithiolates on plasmonic AuNPs and AgNPs that bridges two AuNPs or electrodes as a single molecular linker,[34, 106, 107, 110] conclusions from studies on the organodithiol structure and conformation on AuNPs and AgNPs have been highly controversial. For example, Joo et al proposed that oligomerized dithiols, not dithiol monomers, bridge two plasmonic NPs.[54, 113] This conclusion is drawn from the appearance of a significant S-S feature in the SERS spectra obtained with 1,2-ethanedithiol (EDT) and 1,3-propanedithiol (PrDT) on AuNPs. More recently, we demonstrated (as discussed in chapter two) that *para*-aryl-dithiols (PADT; HS-$(C_6H_4)_n$-SH, n=1,2,3) exist predominantly as monothiolates even in strongly basic solutions (2 M NaOH) and on both AuNPs and AgNPs in water.[114] This conclusion is drawn from the Raman- and SERS-based pH titration study in which the S-H stretch Raman feature remain present in the Raman spectra obtained with basic PADT solutions and SERS samples.

Studying the organothiol binding with colloidal AuNPs and AgNPs is challenging. While there are extensive reports on the organothiol or dithiol interactions with planar gold and silver film, many of these studies were performed under inert environments or organic solvents.[39, 42, 43, 115-121] Extrapolating what has been observed on

the planar gold and silver surfaces to aqueous AuNPs and AgNPs can be problematic because of the complications in the metal structure and solvent polarity in the latter samples. For example, long-chain 1-alkanethiols are highly ordered on planar gold and silver films,[21, 24, 122] but they are mostly disordered on AuNPs.[123] The disorder is due most likely to the AuNP surface curvatures and defects. In contrast, the same 1-alkanethiols on AgNPs can be highly ordered. The latter was attributed to the mobility of the surface silver atoms.[123] Another complication in studying the organothiol interaction with plasmonic NPs is that organothiol can induce spontaneous AuNP and AgNP aggregations. The interplay of ligand adsorption and NP aggregation can cause structure and conformational heterogeneity of organothiols on the AuNP surfaces. This can be especially true for organodithiol interactions with AuNPs and AgNPs. Unlike monothiols that bind to AuNPs as monothiolates by releasing its sulfur-bound hydrogen as proton,[101] organodithiol binding to NPs is much more complicated. It can bind as a monomer on the same NP in both monothiolate and dithiolate forms (Figure 3.1(A)), or as a dithiolate monomer bridging two AuNPs (Figure 3.1(B)). The adsorbed dithiol can also be joined to each other through disulfide bond formation (Figures 3.1(C) and 3.1(D)). These disulfide-linked dithiols can be formed horizontally (intralayer) between two dithiols which are both linked to the same NPs, or vertically (interlayer) between an organodithiol anchored on the NP surface and others extending into solution (Figure 3.1(C)). Finally, the disulfide-linked oligomer's terminal sulfur atoms can bridge two NPs (Figure 3.1(D)). Imaginably, the interplay of the ligand adsorption and NP aggregation events likely plays significant role on the structural and conformational distribution of the organodithiols on

the NP surfaces. This is because aggregation can limit the accessibility of AuNPs and the surface adsorbed thiols.

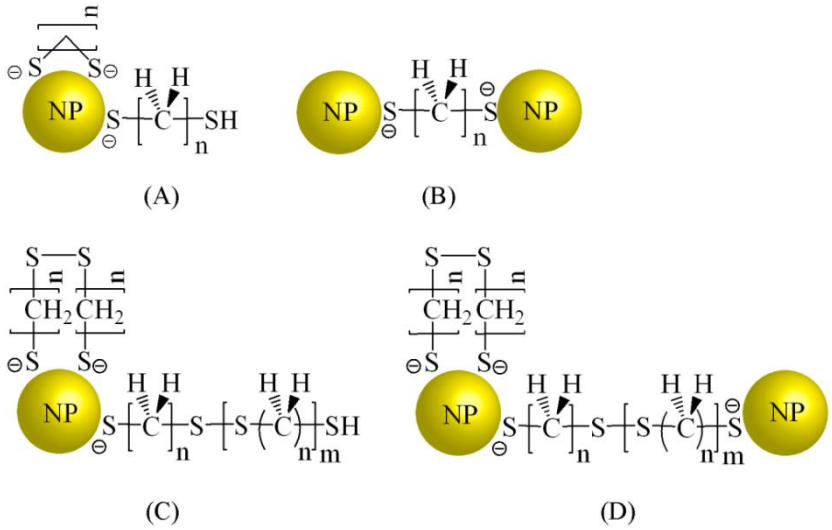

Figure 3.1 Possible structures and conformations of ADTs on AuNPs

SERS have been used extensively for studying the organothiol interactions on plasmonic AuNPs and AgNPs.[124, 125] The apparent absence of characteristic S-H stretching features in the organothiol SERS spectra was often viewed as the evidence for organothiol thiolation.[55, 90, 91] This interpretation can be problematic for organodithiols as has been shown with Raman and SERS study of PADTs in chapter two. Both experimental and computational investigations revealed that deprotonation of one PADT thiol drastically reduces the Raman activity of the remaining thiol making it very easy to misinterpret the PADT monothiolate as dithiolate. Furthermore, SERS can be a highly biased method in that the obtained SERS signal is dominated by molecules that are located in the NP region of highest SERS activity and by the molecules that have high

Raman activity. Therefore, SERS alone is inadequate for providing comprehensive picture of structure and conformation of organodithiols adsorbed onto the NP surface.

The goal of this current study is to determine the structure and compositions of the ADTs adsorbed onto AuNPs and AgNPs in water, using a combination of SERS, ICP-MS, TEM, UV-vis LSPR measurements, and computational simulations. These multi-instrumental analyses offered a series of new insights that would not otherwise be attainable with any of the individual techniques. The model ADTs used in this work are 1,2-ethanedithiol (EDT), 1,4-butanedithiol (BuDT), and 1,6-hexanedithiol (HDT). Alkylmonothiols (AMTs) with the same carbon chain lengths (CH_3 $(CH)_n$-SH, n=1, 3, 5) as the model ADTs were also employed as controls in our LSPR study.

3.3 Experimental section

3.3.1 Materials and equipment

All chemicals were purchased from Sigma-Aldrich. ADTs, AMTs, mercaptoethanol (ME), and disulfide linked mercaptoethanol (2-hydroxyethyldisulfide, (HED)) were purchased and used as received within four months of purchase. The reagent purity are all 95% or above. Nanopure water was used throughout the experiments. The normal Raman and SERS spectra were obtained with a Horiba LabRam HR800 confocal Raman microscope system and a 633 nm Raman excitation laser. UV−visible measurements were taken using an Olis HP 8452 diode array spectrophotometer. TEM analysis was performed on a Joel 2100 instrument. ICP-MS measurements were done using PerkinElmer ELAN DRC II instrument equipped with a dynamic reaction cell (DRC).

3.3.2 AgNP and AuNP synthesis

AuNP and AgNP synthesis was done using the same citrate reduction methods described in the experimental section of chapter two.[18, 94]

3.3.3 Normal Raman and SERS analysis

All the normal Raman and SERS spectra were taken with an Olympus 10× objective (NA = 0.25) and spectrograph grating of 300 grooves/mm. The laser intensity before entering the sample for normal Raman spectra and SERS spectra were 13 and 1.3 mW respectively. The spectral integration time varied from 5 to 50 s. The Raman shift was calibrated with a neon lamp, and the Raman shift accuracy was ~0.5 cm^{-1}. The normal Raman spectra of the ADTs were acquired using the neat liquid samples. The ADT solutions were prepared from stock (1 mM in ethanol) by serial dilution with water.

3.3.4 pH changes induced by ADT adsorption onto AuNPs

Molecular adsorbates such as citrate ions on AuNP can interfere with the detection of pH change associated with ADT adsorption onto the AuNPs. These adsorbates were removed through combination of KCl-induced AuNP aggregation followed by washing with water. Briefly, KCl (0.4 g) was added to 40 mL of the as-synthesized AuNPs to induce aggregation. The supernatant was removed and the AuNP aggregates were washed 6 times, each with 40 mL of water until the pH of the washing solution is constant. The AuNP aggregates were transferred into 2 mL Eppendorff tube and all the supernatant removed. 1 mL of 1 mM BuDT in 50% ethanol was added to the aggregates and vortexed. The pH of the supernatant on the AuNP aggregate was monitored over time. The pH of 1 mM BuDT in 50% ethanol was also taken as control.

3.3.5 ICP-MS measurement of S/Au ratio

The S/Au ratio for the AuNP/ADT or AuNP/AMT aggregates was determined using ICP-MS. Briefly, excess ADT or AMT was added to the AuNP solutions. The mixtures were left overnight to allow AuNP aggregation and settling. The ADT- and AMT-containing NP solutions were then split into two equal volume fractions in which only the bottom fraction contains NPs. An equal volume of aqua regia was added to both fractions to digest the NPs. The digestion solutions were further diluted with Nanopure water prior to the MS analysis. The amount of ADT or AMT adsorbed onto the NPs was determined on the basis of the difference in the sulfur content between the top and bottom fractions. The sulfur concentrations were analyzed using ICP-MS in the DRC mode. A calibration curve for sulfur content from 0 to 1750 ppb was established for ICP-MS analysis using zinc sulfate as standard. The Au content in the solution was also analyzed in the standard mode. A calibration curve for the Au analysis from 0 to 39400 ppt was constructed using a ICP-MS Au standard obtained from Sigma Aldrich.

3.3.6 UV-vis measurements of the AuNP LSPR

The time-resolved UV-vis measurements were performed to study the AuNP LSPR shift associated with ADT- and AMT-induced AuNP aggregations. Briefly, 1 mL of AuNPs was mixed with equal volume of water followed by the addition of 1 mL 0.1 mM of ADT or AMT. The mixtures were stirred continuously during the time-resolved measurements. The time-interval between consecutive spectral acquisitions was 1 min.

3.3.7 TEM analysis

The TEM images for the ADT-containing AuNP and AgNP aggregates were acquired for the precipitates in AuNP/ADT and AgNP/ADT mixtures after 4 days of sample incubation. Possible free ADT in the sample mixtures was removed before TEM measurements by washing the precipitates three times with Nanopure water. TEM images were taken with Cu grids covered with a Formvar carbon film at an accelerating voltage of 200 kV. The nominal concentration of ADT in the samples used for TEM imaging was 33 μM.

3.3.8 Computed Raman spectra of intact EDT and EDT monothiolate

All the quantum calculations were performed by Gaussian 09 suite. The ground state structures of the EDT were optimized using density functional theory (DFT) method with BP86 functional at the level of 6-311++G (d, p) basis set. Frequency analysis was carried out and no imaginary frequencies were found, ensuring that all of the structures were stable. The Raman spectra were calculated based on these optimized structures using the same functional and basis set as geometry optimization. The calculated wavenumbers in Raman spectra were not scaled by any factor. The Raman intensity ratio of S-H stretch (~ 2590 cm^{-1}) to C-C stretch (~ 1275 cm^{-1}) in the computed spectrum reduces from 12 for intact EDT to 3.0 for EDT monothiolate, indicating that the relative Raman activity of the remaining S-H in the EDT monothiolate is only 2 times lower than that of the average S-H Raman activity in intact EDT.

3.3.9 Computational modeling of LSPR of AuNP aggregates as a function of AuNP gap sizes.

The T-matrix method was used to calculate the extinction spectra of AuNP aggregates with different spacing between AuNPs.[126] In the calculations, the coordinates of the AuNPs were generated using Monte Carlo method. The first particle was placed at the origin of the coordinate, the following particle coordinates are generated using Monte Carlo method and their distance with the previous particles are kept above a fixed minimum value. For example, if the minimum distance was fixed at 1.4 nm, the distance between the first and the second particle is 1.4 nm, the distance between nth and (n+1)th particles is also kept at 1.4 nm, however, the distances between (n+1)th particle with all other particles are always over 1.4 nm so that the generated aggregate is similar to the experimentally generated amorphous structure. Once the coordinates of particles were generated, their interaction and extinction spectra were calculated using T-matrix method. In the simulations, the distance was varied from 1.4 nm to 4.28 nm. In the experiments, the diameter of the particles is 13 nm, over several thousands of particles were required to simulate the comparable size of the aggregate which is not affordable using our computer resource. We used particles with diameter of 50 nm to show the trend in the spectra change when the interparticle distance is changed. Only 50 particles are required to generate extinction spectra with resonance wavelength ranging from 700-800 nm.

3.4 Results and discussion

3.4.1 ADT binding with AuNPs

Addition of the ADTs into the aqueous AuNPs induces immediate AuNP aggregation and complete settling after ~2 h of sample incubation (Figure 3.2). This

occurred even when the nominal ADT concentrations in the AuNP/ADT solution were as low as 3 μM. This value is far below the threshold concentration of ~10 μM for ADT to form a full monolayer packing capacity on the AuNPs. This threshold concentration was estimated by assuming the AuNPs are perfectly monodispersed with diameter of ~13 nm, spherical, and the full monolayer ADT packing density is similar for the reported alkanethiols on planar gold film (0.77 nmol/cm^2).[127]

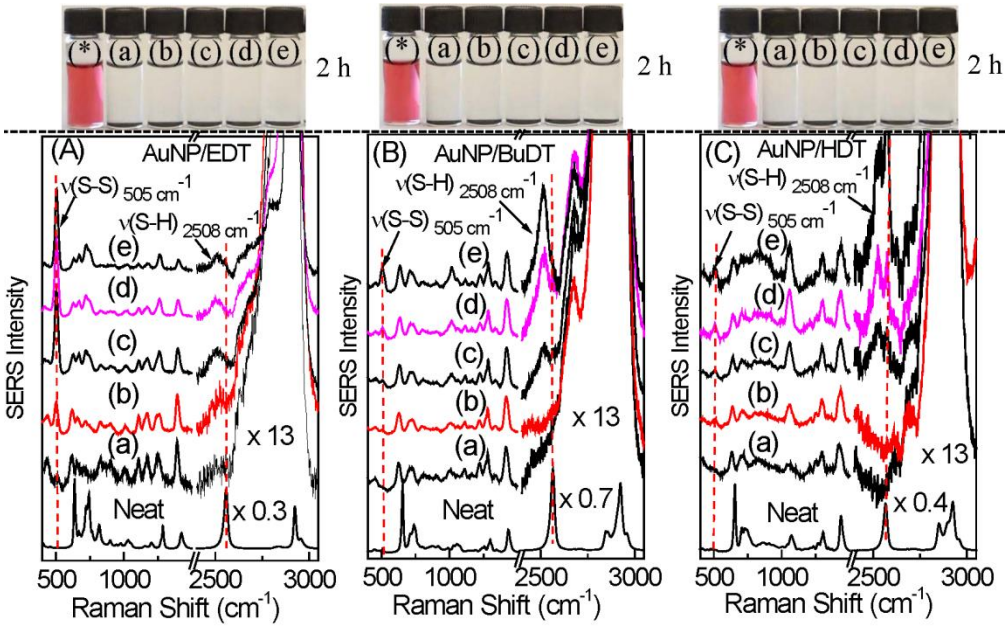

Figure 3.2 (*Upper row*) Photographs of AuNP/ADT mixtures with different concentrations of ADTs after 2 h of sample incubation. (*Bottom row*) Representative SERS spectra of samples shown in the photograph for (A) EDT, (B) BuDT, and (C) HDT on AuNPs.

Note: The nominal concentrations of ADTs in sample (a)-(e) are 3 μM, 10 μM, 25 μM, 50 μM, and 250 μM respectively. The concentration of AuNPs in the samples is ~4 nM. The concentration of the AuNPs was estimated using the extinction coefficient of 2.7 $\times 10^8$ M^{-1} for 13 ±1.3 nm particle diameter, assuming the AuNPs are monodispersed. The AuNP size was obtained from an average size of 56 particles. The SERS spectral features in the region from 2400 cm^{-1} to 3100 cm^{-1} are magnified by the specified factors. The dotted lines in (A-C) indicate the expected positions for S-S and S-H peaks.

SERS spectra obtained with the aggregated AuNPs revealed that the degree of ADT thiolation and disulfide formation on AuNPs depends not only on the ADT concentrations, but also the ADT carbon-chain length. At submonolayer concentrations, the ADTs exist predominantly as dithiolate forms on AuNPs. The S-H stretching feature in the ~2600 cm^{-1} region that is prominent in the ADT normal Raman spectra entirely disappeared in the samples containing 3 μM ADTs. However, when the ADT concentrations approach, are equal to or higher than 10 μM, both disulfide stretching (S-S, ~505 cm^{-1}) and S-H stretching features appeared in the ADT SERS spectra. pH measurement confirms that protons were released when ADT binds to AuNPs. The pH of supernatant of the AuNP/BuDT aggregate changes from 6.09 to 4.38 after BuDT adsorption (Table 3.1). This is consistent with the conclusion that organothiols bind to AuNPs primarily as thiolates by releasing the sulfur-bound hydrogen as a proton.[101]

Table 3.1 pH of supernatant of AuNP/BuDT aggregate during BuDT adsorption

Time (min)	pH of supernatant
0 (control)	6.09
5	4.40
15	4.38
30	4.38
1440	4.38

pH of 1 mM BuDT in 50% ethanol (control) is 6.09

Importantly, using the detectability of S-H SERS feature to gauge the degree of ADT thiolation was validated with computational modeling. The modeling indicates that deprotonation of one ADT thiol has no significant impact on Raman activity of its remaining thiol relative to other spectral feature such as C-C stretching feature in the ~1275 cm^{-1} region (Figure 3.3).

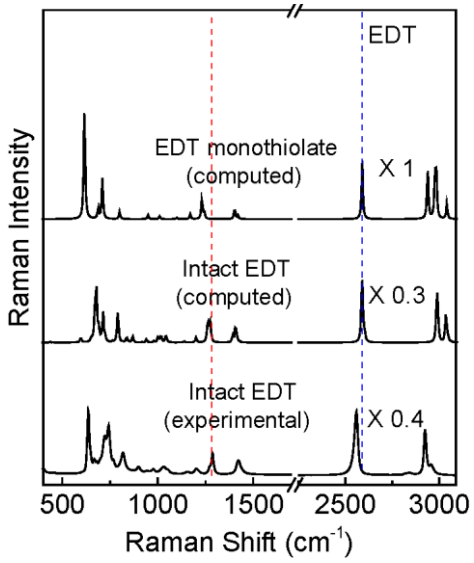

Figure 3.3 Experimental Normal Raman spectra of intact EDT, and computed Raman spectra of intact EDT and EDT monothiolate.

The experimental normal Raman spectrum was acquired with neat EDT. The dotted lines from left to right are the peak positions for C-C stretch ($\nu_{C\text{-}C}$) and S-H stretch ($\nu_{S\text{-}H}$) respectively.

This is in sharp contrast to PADTs (discussed in chapter two) for which deprotonation of the first one thiol drastically reduces the Raman activity of the remaining thiols.[114] Taking the experimental spectrum of 1,4-benzenedithiol (BDT), the simplest PADT, as an example, deprotonation of one BDT thiol reduces the Raman activity of its remaining thiol by ~50 times relative to the BDT C-C stretching feature. This difference between ADT and PADT indicates the critical importance of the junction R group on the chemical reactivity between the first and second thiol in organodithiols (HS-R-SH).

The Raman intensity ratio between the S-S and S-H features can be used for estimating the concentration ratio of distal thiols of ADTs on AuNPs that are disulfide-linked or remains as intact thiol group, assuming the SERS enhancements experienced by

these two functional groups are the same. The normal Raman cross-section ratio between S-S and S-H is 1.66, which is determined on the basis of Raman spectra of HED and mercaptoethanol itself (Figure 3.4). The normal Raman cross section ratio ($\frac{\sigma_{S-S}^{513}}{\sigma_{S-H}^{2586}}$) is determined using the equation below (3.1)

$$\frac{\sigma_{S-S}^{513}}{\sigma_{S-H}^{2586}} = \frac{I_{S-S}^{513}}{I_{S-H}^{2586}} \times \frac{C_{ME}}{C_{HED}} \tag{3.1}$$

Where I_{S-S}^{513} and I_{S-H}^{2586} are the Raman intensities of HED and ME peaks at ~513 cm^{-1} and ~ 2586 cm^{-1} respectively in Figure 3.4 (a) and (b) respectively. C_{HED} and C_{ME} are the concentrations of HED and ME in the sample mixtures shown in Figure 3.4 (a) and (b) respectively.

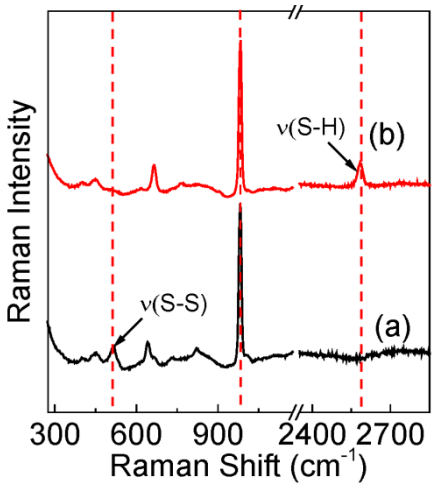

Figure 3.4 Normal Raman spectra of (a) HED/ Na_2SO_4 and (b) ME/ Na_2SO_4 mixture.

Note: Na_2SO_4 was used as internal reference and the peak for SO_4^{2-} at ~983 cm^{-1} is normalized in both spectra. The nominal concentration of HED and ME in the mixtures is 150 mM. The dotted lines from left to right in the plot represent the peak positions for S-S and S-H respectively.

Using the SERS spectrum (e) shown in Figures 3.2 (A), 3.2 (B), and 3.2 (C), the estimated number of S-S is 34**,** 1.6**,** and 1 times that of S-H bonds in EDT, BuDT, and HDT on AuNPs, respectively. This result indicates that the distal thiols in EDT are drastically more extensively disulfide-linked than those in both BuDT and HDT. Indeed the S-H features are barely visible in the EDT SERS spectra, but much more prominent in the equally magnified BuDT and HDT SERS spectra.

The disulfide bonds observed in the ADT SERS spectra on AuNPs are formed after ADT were adsorbed onto AuNPs. No detectable S-S Raman features were observed in any of as-received ADTs (Figure 3.2). Indeed, if those disulfide bonds in the SERS samples are from the disulfide-linked ADT impurities in the as-received reagents, the amount of the S-S is likely independent of the ADT carbon-chain length. Presumably, the carbon-chain length should not have a significant effect on the reaction kinetics of the ADT disulfide formation reactions in solution.

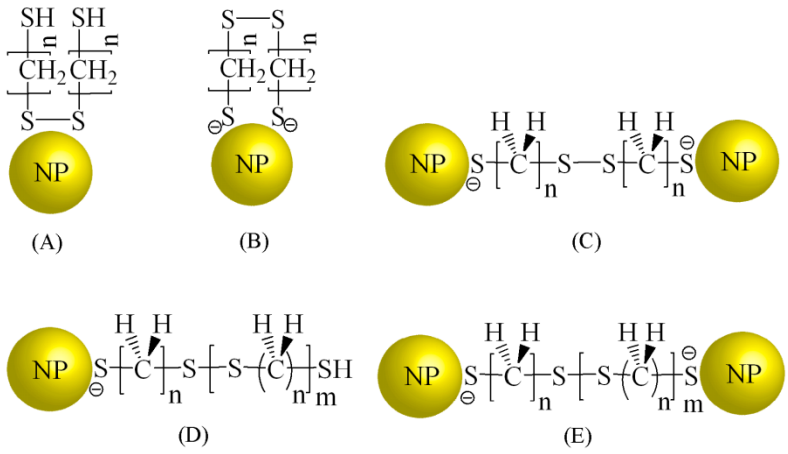

Figure 3.5 Possible structures of the disulfide-linked ADT on AuNPs.

Monothiols on planar gold film were proposed to form disulfide-linking between the sulfur atoms at the gold and thiol interfaces.[128] This raises the possibility that disulfide bonds seen for the ADTs on AuNPs (Figure 3.2) are formed between the α-thiols that are the thiols at the AuNP/ligand interfaces (Figure 3.5A). This possibility was excluded on the extensive SERS studies of monothiol adsorption onto AuNPs in which no S-S stretching features have been observed.[31, 123, 129] This configuration also does not agree with the observation of a control experiment conducted with HED on AuNPs. No S-S stretching SERS feature was observed when HED was adsorbed onto AuNPs despite the strong S-S Raman intensity in the HED normal Raman spectrum (Figure 3.6). These experimental data confirmed that the disulfide observed for ADTs on AuNPs is formed exclusively from the distal thiol group of the ADT anchored on AuNPs, but not the α-thiol shown in Figure 3.5A.

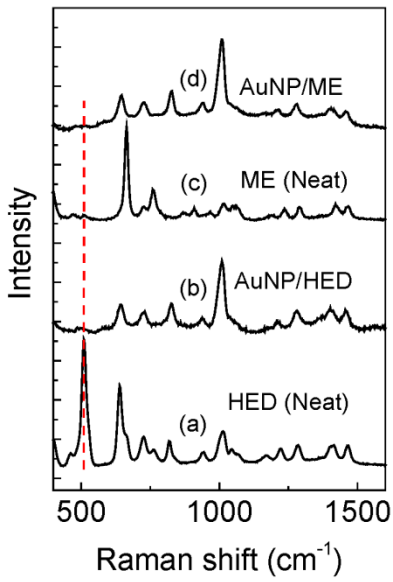

Figure 3.6 (a, c) Normal Raman spectra of HED and ME respectively, and (b,c) their SERS spectra on AuNPs respectively.

Note: The nominal concentration of HED and ME in the SERS samples is 33 μM. The normal Raman spectra were obtained for the neat samples. The dotted line in the plot represents the peak position for S-S. SERS results show that HED adsorbs dissociatively through breaking of the S-S bond as evidenced by the close resemblance of the AuNP/ME and AuNP/HED SERS spectra.

There are four possible configurations for the disulfide bonds formed by the distal ADT thiols (Figures 3.5(B) to 3.5(E)). i) intralayer (horizontal) coupling between the two ω-thiols on two adjacent ADT molecules adsorbed on the same NPs (Figure 3.5B), ii) vertical coupling between two ω-thiols each in a ADT molecule that is attached to a different AuNP (Figure 3.5C), iii) S-S formation through interlayer coupling between the ω-thiol of the ADT directly anchored on the AuNPs and an -SH of ADT free in solution (Figure 3.5D), iv) S-S formation in oligomerized or polymerized ADTs that crosslink two NPs (Figure 3.5E). Much experimental evidence supports the hypothesis that formation of the disulfide linkage proceeds primarily through intralayer coupling (Figure 3.5B), but not through the interlayer-linking as suggested by Joo et al.[54] ICP-MS comparison of the

sulfur attached to AuNP in EDT-, BuDT-, HDT-containing AuNP aggregates after overnight sample incubation is 1.0 ± 0.1, 0.8 ± 0.1, 0.60 ± 0.02 times of that attached to the monothiol 1-butanethiol (BuT) functionalized AuNP aggregate (Table 3.2).

Table 3.2 Comparison of S/Au ratio of BuT/AuNP, EDT/AuNP, BuDT/AuNP, and HDT/AuNP determined using ICP-MS.

Sample	S/Au	S/Au / $(S/Au)_{BuT}$
AuNP/BuT	0.05 ± 0.001	1 ± 0.03
AuNP/EDT	0.05 ± 0.007	1 ± 0.1
AuNP/BuDT	0.04 ± 0.004	0.8 ± 0.1
AuNP/HDT	0.03 ± 0.001	0.6 ± 0.02

The S/Au ratio should be significantly higher for the ADT-containing AuNPs than that for BuT-containing AuNPs if there is substantial vertically disulfide-linked ADT on AuNPs. This is because BuT contain one sulfur and can bind only as a monolayer onto AuNPs.

The intralayer cross-linking hypothesis is also supported by rapid formation kinetics of S-S bond when EDT was added into the aqueous AuNP. An intense S-S stretching SERS feature was observed within the first ~10 min of the sample mixing, which is the measurement dead time for the first SERS acquisition (Figure 3.7). This is exceedingly fast considering the fact that only 10 μM EDT was added into the AuNP solution. Such rapid S-S formation is too fast for the vertical sulfide bond formation that occurs between a EDT molecule anchored on the AuNPs and one remaining free in solution. First, the diffusion coefficient of the AuNPs together with the surface adsorbate should be very slow, that reduces the reaction between EDT on AuNPs and that in solution. Second, the nominal EDT and AuNP concentrations in the EDT/AuNP solutions are 10 μM and 4 nM, respectively. Such concentrations are exceedingly low for effective

S-S formation between EDT on AuNP and that in solution. Indeed, the average actual EDT and AuNP concentrations during the EDT adsorption process in the EDT/AuNP solution must be significantly lower than their respective nominal concentrations due to the ligand adsorption and AuNP aggregations. Compared to the disulfide bonding between a EDT molecule on AuNP and one in solution, EDT binding to AuNP is much faster because of the large number of surface gold atoms.

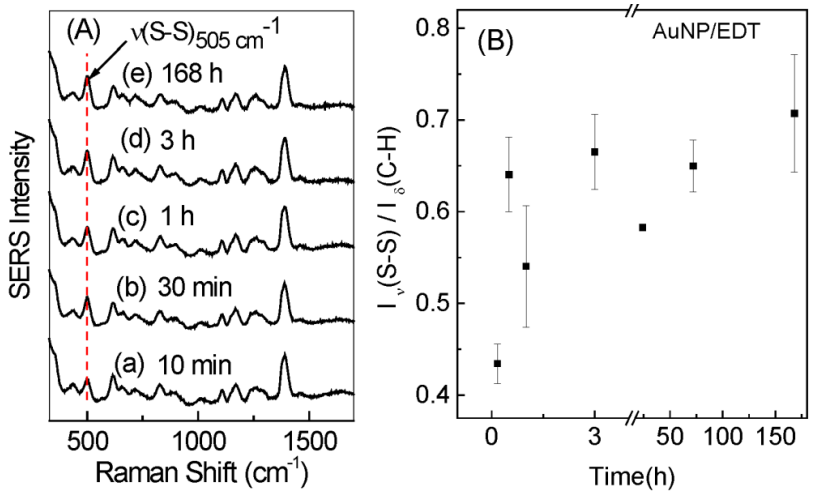

Figure 3.7 (A) Time dependent SERS spectra of AuNP/EDT. (B) Plot of the intensity ratio of S-S to C-H bending as a function of time.

Note: The nominal concentration of EDT in the samples is 10 μM. The error bars represent one standard deviation from three independent measurements.

Two reasons can explain why EDTs anchored on AuNP can rapidly form intralayer disulfide cross-linking among themselves. The first is that ligand adsorption rapidly increases the EDT local concentration on the AuNP surface. This concentrating process reduces the rate of vertical EDT disulfide formation, but enhances the rate of intralayer disulfide-bond formation. Secondly, all the EDTs anchored perpendicular to AuNP surfaces have their distal end thiol groups confined in close proximity. This

facilitates intralayer disulfide formation among the ADTs, as long as the distal thiols are close enough to covalently bond.

The ICP-MS comparison of S/Au ratio of ADT-functionalized AuNPs with that for the BuT-functionalized AuNPs is revealing. The S/Au ratio for the ADT-functionalized AuNP should be approximately twice of that for BuT-functionalized AuNPs if all ADTs bind vertically as a monolayer onto AuNPs, regardless of the ADT carbon-chain lengths. On the other hand, the S/Au ratios of the ADT-functionalized AuNPs are carbon-chain length dependent if these ADTs lie flat on the AuNPs. The S/Au ratio of EDT-, BuDT-, and HDT-containing AuNPs should be 1/4, 1/6, and 1/8 times that of BuT-containing AuNPs, respectively, assuming that all ADTs are lying flat in a fully extended conformation. The fact that experimental S/Au ratio are between the predicted values for the vertically and flat-lying ADTs indicates that ADTs on AuNPs are mixture of flatly and vertically bounded ones. The vertical ADTs are responsible for the S-S and S-H stretching features seen in ADT SERS spectra. Unfortunately it is currently impossible to quantify the fraction of the ADTs that are lying flat or standing up.

One common assumption in ADT molecular electronics, SERS, and quantum plasmonic coupling applications is that ADTs bridge two plasmonic nanoparticles via dithiolate-linking in which each sulfur is attached to a different NP. While such conformation is clearly achievable with a carefully controlled sequential ADT and AuNP assembly process as it has recently been demonstrated by Yoon et al,[106, 108] cross-linking two NPs simply by mixing ADT with AuNPs or AgNP is difficult to be achieved and verified. Indeed, experimental determination of the structure of molecules located at NP junctions is challenging. This is because the number of the molecules that actually define

the NP junction size between two adjacent NPs in NP aggregates is very small in comparison to the total number of ADT molecules adsorbed onto the AuNP surrounding areas. In this work, the NP gap size and the structure of ADT junction molecule in the ADT-containing AuNP aggregates is probed by cross-comparing AuNP LSPR peak shifts associated with the AuNP aggregation triggered by ADTs with the corresponding peak shifts caused by AMTs that have the same carbon-chain length (Figure 3.8).

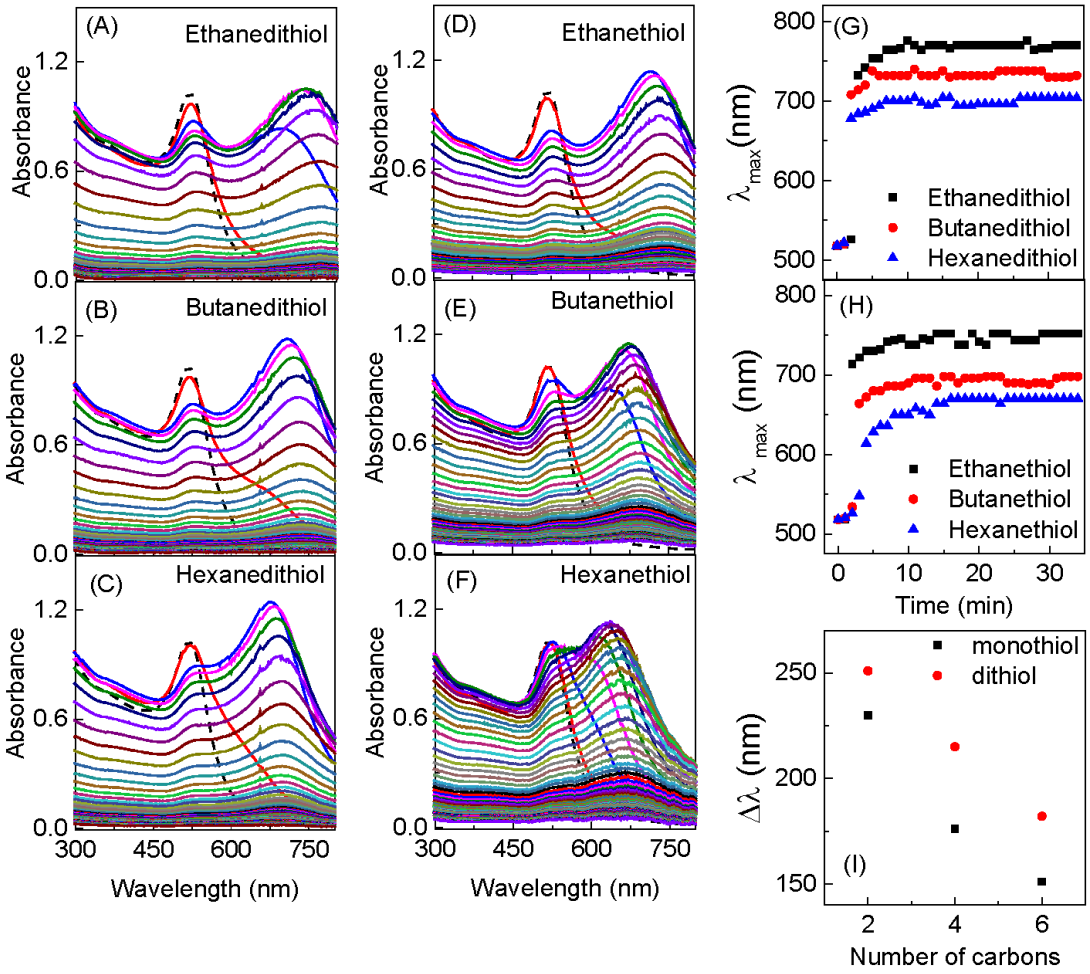

Figure 3.8 Time-resolved UV-vis spectra of (A-C) ADTs and (D-F) AMT on ~13 nm AuNPs. (G, H) Plot of maximum wavelength as a function of time for AuNP/ADTs and AuNP/AMTs respectively. (I) Plot of wavelength shift ($\Delta\lambda$) as a function of the number of carbon chains for dithiols and monothiols.

Note: The final nominal concentration of organothiols in the sample mixtures is 33 μM. The final concentration of the ~13 nm AuNPs in the sample mixtures is ~ 4 nM. The concentration of the AuNPs was calculated using the extinction coefficient of 2.7×10^8 M^{-1} for ~13 nm particle diameter and assuming the AuNPs are monodispersed. The wavelength shift was calculated as the difference between the maximum wavelength at steady state and the wavelength of the AuNP at time t = 0 min.

Additions of ADTs and AMTs invariably induce immediate AuNP aggregations, which are evident from the appearance of a new AuNP LSPR peak that is red-shifted in comparison to the AuNP monomer peak around 520 nm. The degree of the AuNP LSPR

red shift increases with longer sample incubation time for the first few minutes, indicating the growing extent of AuNP aggregation and plasmonic coupling. However, after 10 min or so, the LSPR peak wavelength associated with the aggregated AuNPs becomes constant, while the peak intensity decreases monotonically with sample incubation time. This reduced intensity is due to the agglomeration and precipitation of the aggregated AuNPs.

Two scenarios could lead to constant LSPR peak positions of the aggregated AuNPs. First, AuNP LSPR is sensitive only to initial AuNP aggregation in that appreciable AuNP LSPR shift occurs only before the number of AuNPs in AuNP aggregates reaches a certain threshold value. Further AuNP-aggregate size increases have no detectable effect on the AuNP LSPR feature. Secondly, a AuNP aggregate loses its dispersion stability in water once it grows to certain size. In this case, the AuNP aggregate precipitates without contributing to the measured AuNP LSPR red-shift. Experimental determination of the exact reason why the red-shift of the aggregating AuNPs stops at a constant value is currently impossible because of the difficulty in pinpointing the size and morphological distributions of the aggregated AuNPs in solution. Regardless, the threshold value of the number of AuNPs in the ligand-containing AuNP aggregates to reach steady-state LSPR wavelength should be approximately independent of ADT and AMT carbon-chain lengths. Therefore, the differences in the steady-state LSPR peak wavelengths among the different samples (Figure 3.8) are indicative of the average junction sizes between adjacent NPs in the AuNP aggregates.

Figure 3.8 showed that the shorter the carbon-chain length becomes, the more significant is the AuNP LSPR red-shift associated with AuNP aggregates induced by

either ADTs or AMTs. This carbon-chain length dependent red-shift data confirms that AuNP LSPR peak shift can be used as a molecular ruler for estimating the average gap size of the aggregated AuNPs.[130-133] Indeed, computational simulation, conducted for aggregates each containing 50 AuNPs, showed that the smaller AuNP gap size, the larger LSPR shift of the aggregated AuNPs (Figure 3.9).

Importantly, the AuNP LSPR red-shift induced by EDT, BuDT, and HDT are invariably larger than that induced by ET, BuT, and HT respectively. This indicates the gap size in ADT-containing AuNPs is smaller than that in the AuNPs containing their respective AMT counterparts. This observation is particularly noteworthy because, when both are in extended conformer, ADT is invariably larger than its corresponding AMT on AuNPs. These data excluded the possibility that there are substantial amount of ADTs are in upright conformer in the NP junction areas.

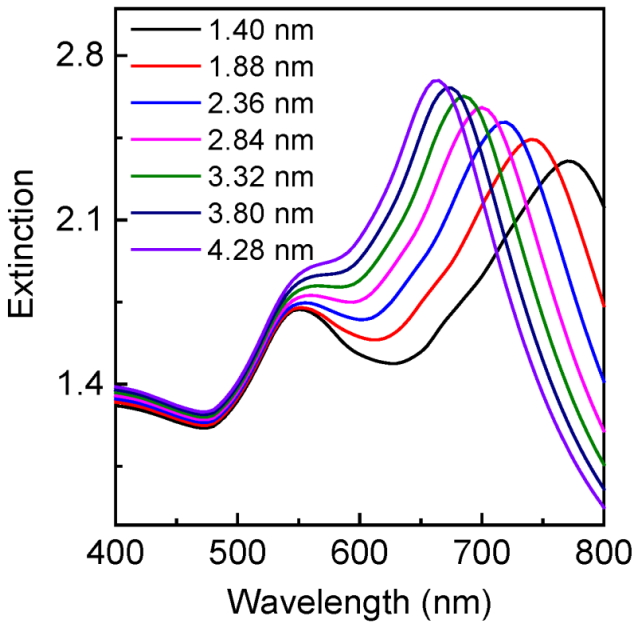

Figure 3.9 Computational simulation for the LSPR shift of AuNP aggregates as a function of the AuNP gap sizes.

Note: The particle diameter of AuNP is 50 nm and the total number of AuNPs is 50.

The cross-comparisons of the AuNP LSPR features associated with AuNP aggregation induced by ADTs and AMTs in Figure 3.8 is revealing. The strong alkyl carbon chain-length dependence of the AuNP LSPR shift associated with the organothiol-induced AuNP aggregation indicates that there must be bound ligands present in the junction area between the adjacent NPs. This, in turn indicates that substantial amount of AMT and ADT adsorption occurs before the onset of the AuNP aggregations. If this was not the case, the AuNP LSPR should be more or less independent of the alkyl chain-length. If the AMTs or ADTs only packed sparely on the AuNP junctions, the strong inter-particle van der Waals forces should compress the few junction molecules present into a totally flat conformer, making the interparticle distance independent of the alkyl chain-length.

The maximum gap size between two adjacent AMT-containing AuNPs in a AuNP aggregate is two AMT monolayers that are both in upright position (Figure 3.10). Since an ADT is longer than its corresponding AMT by a –SH group, these LSPR data allow us to exclude the possibility that there are any significant amount of vertically linked ADTs in the junction areas (Figure 3.10(E)) as proposed by Joo et al, or significant intralayer linked ADTs (Figure 3.10(D)). This is because the gap size between the AuNPs in Figures 3.10 (D) and 3.10 (E) has to be larger than that for the AMT thiol on AuNPs. On the other hand, the structures and conformations depicted in Figures 3.10 (B), and 3.10 (C) fit the existing data and are both possible for ADTs located in the AuNP junctions. This hypothesis is consistent with the S/Au ratio determined with the ICP-MS measurements.

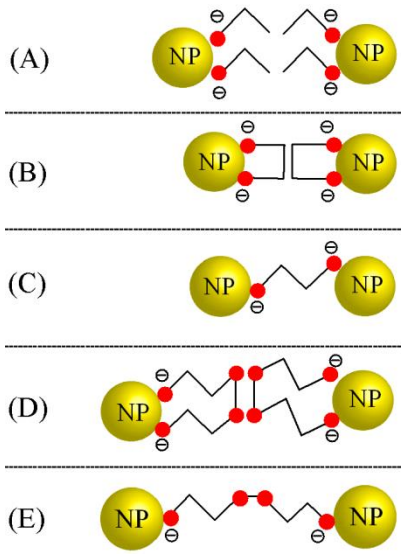

Figure 3.10 Possible structures and conformations of ADT on AuNPs that have comparable gap sizes with monolayer AMT-containing AuNPs, using EDT as the model molecule.

Note: (A) a monolayer of ethanethiol (a monothiol) between two AuNPs, (B) two EDT monomers adsorbed on two different AuNPs as dithiolates, (C) EDT monomer linking two AuNPs as dithiolate, (D) EDT linker molecules having their terminal –SH groups forming S-S bond and (E) dimerized EDT acting as linker between two AuNPs. The red dots in the images represent sulfur atoms.

Taking all the results from SERS, ICP-MS, and LSPR measurements into consideration together, it is evident that ADTs on AuNP surfaces are mixtures of multiple structures and conformations. The exact structure and conformation of ADTs on AuNP depends not only on the ADT carbon-chain lengths and concentrations, but also on ADT locations on the AuNPs (junction or surrounding). For example, the extensive S-S stretching feature observed in EDT SERS spectra is likely from the molecules that are located outside of the junction areas. This is because the horizontal disulfide-linkage between the surface-bound ADTs likely occurs in area where ADTs can be densely

packed, while the vertical disulfide-linkage between ADT directly anchored on AuNPs and that extended in solution should only be possible in which ADT molecules are free to diffuse in and out. However, the ADT packing density and accessibility in NP junction areas must be lower than their respective counterparts for ADTs outside the junction regions.

3.4.2 ADT binding with AgNPs

ADT binding to AgNPs is significantly different from that to AuNPs. First, ADT binding induces immediate AuNP aggregations, and complete AuNP settling within the first two hours of ADT mixing with AuNPs. However, no appreciable AgNP settling occurred in the ADT/AgNP mixing within the first 3 h of the sample preparations (Figure 3.11). It took more than 10 days for the AgNPs in all the ADT/AgNP mixtures to settle to the bottom of the sample vials.

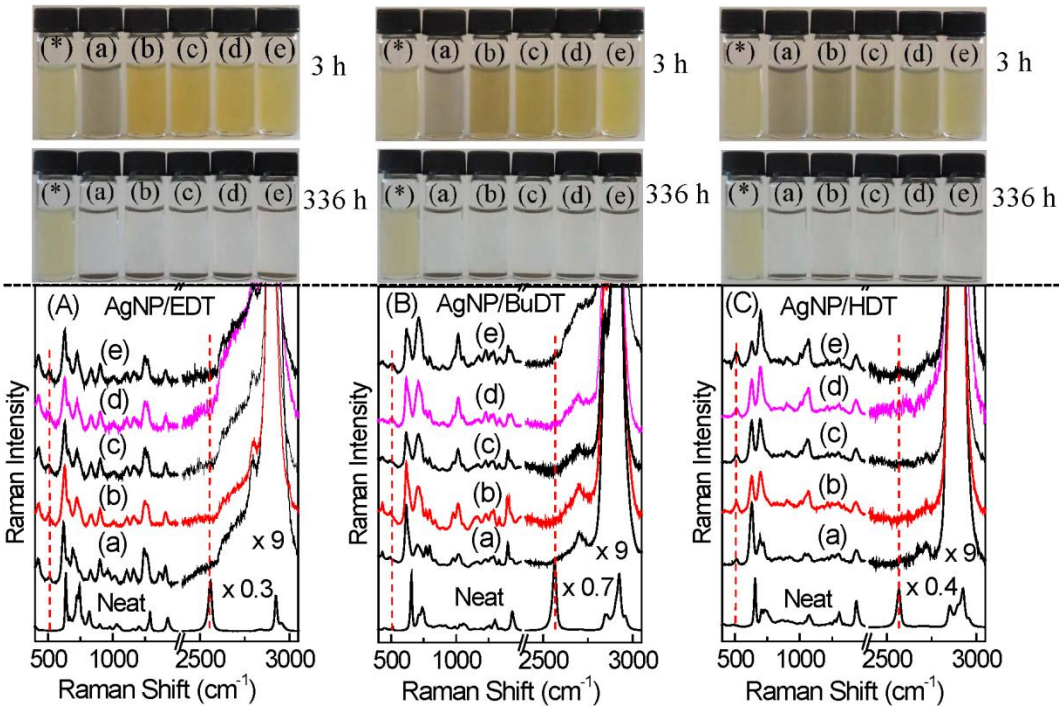

Figure 3.11 (*Top row*) Photographs of AgNP/ADT mixtures with different concentrations of ADTs after 3 h and 336 h of sample incubation. (*Bottom row*) Representative SERS spectra of the samples shown in the photograph for (A) EDT, (B) BuDT, and (C) HDT on AgNPs.

Note: The samples were prepared by mixing 1 mL of twice diluted AgNPs and 1 mL of water followed by 1 mL of ADT. The nominal concentrations of ADTs in samples (a)-(e) are 3 μM, 10 μM, 25 μM, 50 μM, and 250 μM, respectively. The spectral features in the region from 2400 cm^{-1} to 3100 cm^{-1} are magnified by the specified factors.

Second, TEM measurements revealed that ADTs induce significant AgNP disintegration **(**Figure 3.12) in which large amounts of amorphous precipitate appear in the TEM image obtained with the washed precipitate in the ADT/AgNP mixture. No such NP disintegration was observed in the ADT/AuNP mixtures that are aged for the same period of time (Figure 3.13). Third, SERS spectra obtained with the precipitates in the ADT/AgNP mixtures are also remarkably different from those acquired from precipitates in their corresponding ADT/AuNP mixture (Figures 3.2 and 3.11). The C-S stretching SERS intensities of C-S *gauche* ($I_{\nu(C\text{-}S),G}$) at the ~620 cm^{-1} region and *trans* C-S ($I_{\nu(C\text{-}S),T}$)

at ~690 cm^{-1} region in the ADT/AgNP mixtures are significantly more intense than in their respective ADT/AuNP counterparts. Moreover, the intensity ratio of C-S *trans* versus C-S *gauche* SERS features increases with increasing ADT concentrations in the ADT/AgNP mixtures as shown by the plot in Figure 3.14, but remained approximately unchanged for the ADT/AuNP mixtures (Figure 3.2).

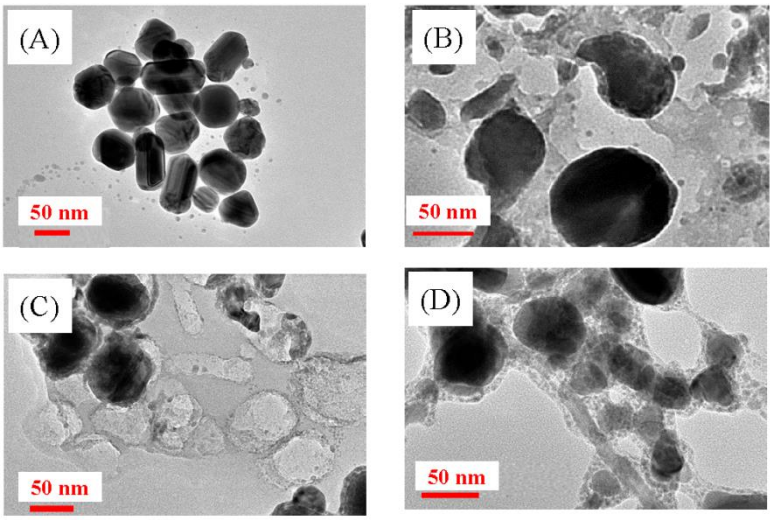

Figure 3.12 TEM images of (A) AgNP, (B) AgNP/EDT, (C) AgNP/BuDT, and (D) AgNP/HDT.

Note: The samples were prepared by mixing 1 mL of two times diluted AgNP with 1 mL water followed by 1 mL of the ADT. The concentration of ADT in the TEM samples is 33 μM. The TEM images were taken after 4 days of sample incubation.

Comparing and contrasting ADT versus AMT for their binding to AgNPs proves to be quite instructive. We recently reported a comparative study of AMT binding to AgNPs versus AuNPs in which the model AMT carbon-chain lengths vary from 2 to 14. With ethanethiol the only exception, the AMTs on AgNPs are almost exclusively in C-S *trans* conformer.[123] This differs from ADTs on AgNPs where both C-S *trans* and *gauche* conformers are present. This indicates that the AMTs are more highly ordered on AgNPs

but mostly disordered for ADTs. Furthermore, no significant AgNP disintegration occurred even after one month of incubating the AMT/AgNP mixtures. This stands in sharp contrast to the ADT-induced AgNP disintegration. This AgNP disintegration is caused by ambient oxygen oxidizing surface silver atom and the organodithiol then accelerates the AgNP disintegration by chelating the oxidized silver.[102]

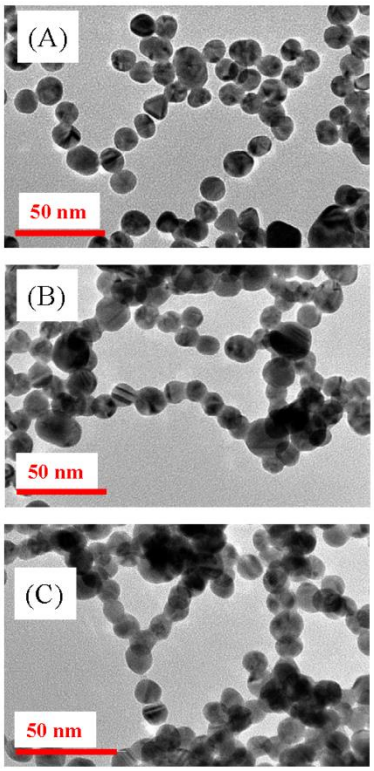

Figure 3.13 TEM images of (A) AuNP/EDT, (B) AuNP/BuDT, and (C) AuNP/HDT.

Note: The samples were prepared by mixing 1 mL of AuNP with 1 mL water followed by 1 mL of the ADT. The concentration of ADT in the TEM samples is 33 μM. The TEM images were taken after 4 days of sample incubation.

The fact that AgNP are substantially disintegrated in AgNP/ADT mixtures, but not in their corresponding AgNP/AMT solutions indicates that ADT is not as effective as AMT in passivating the AgNP from oxidative disintegration. This observation is

consistent with the fact that ADT is drastically more disordered than AMT on AgNP surfaces. Therefore, oxygen can readily diffuse through the ADT overlayer and react with silver atoms in AgNPs. The exact reason for the structural and property differences between ADT and AMT on AgNPs is currently unclear. The attempt to determine the structure of the disintegrated AgNP/ADT complex was unsuccessful. Regardless, the TEM data excluded the possibility of ADT linking two AgNPs as a single-molecule dithiolate spacer. The significant NP disintegration observed in the ADT/AgNP mixture strongly suggests that the two ADT thiols have both reacted mostly with Ag^+, but not with intact AgNPs. This conclusion is supported by the SERS spectra in Figure 3.11 that ADTs on AgNP are predominantly in dithiolate form. No significant S-S or S-H stretching features were observed in the SERS spectra obtained with the AgNP/ADT mixtures.

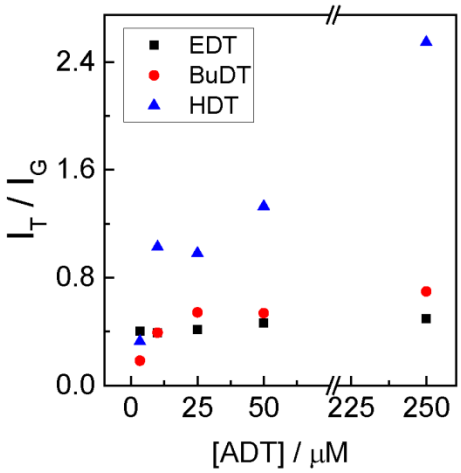

Figure 3.14 Intensity ratio of C-S *trans* (T) to C-S *gauche* (G) as a function of the nominal ADT concentration.

Note: The ratio is determined from the SERS spectra of ADT on AgNPs.

3.5 Conclusions

ADT interactions with AuNPs are significantly different from its binding to AgNPs. The ADT thiol groups at the AuNP/ligand interface are in thiolate form in which the sulfur-bound hydrogen is released as a proton. The remaining thiol can either remain intact, generate a disulfide bond with another ADT, or become deprotonated by attaching to the same or a different AuNP. ICP-MS measurements reveal that some ADT molecules lie flat on AuNPs. The degree of the disulfide bond formation of the upright ADTs on AuNPs depends critically on the carbon chain-length. EDTs are more extensively disulfide-linked compared to BuDT and HDT molecules on AuNPs. The gap size in the ADT-containing AuNP aggregates is significantly smaller than that in AuNP aggregate counterparts that contain AMTs of the same carbon-chain length. This excludes the possibility that significant amount of oligomerized ADTs are present at the AuNP junctions. In sharp contrast to the structural complexity of ADT on AuNPs, ADT induces significant AgNP disintegration during which ADTs were converted predominantly to dithiolate. The insights from this study will be important for developing a comprehensive understanding of organodithiol interactions with the plasmonic AgNPs and AuNPs in water.

Notes: This work has been previously published: Gadogbe, M.; Zhou, Y.; Alahakoon, S. H.; Perera, G. S.; Zou, S.; Pittman, C. U.; Zhang, D., Structures and Conformations of Alkanedithiols on Gold and Silver Nanoparticles in Water. *J. Phys. Chem. C* **2015,** *119*, 18414-18421.

REFERENCES

1. Anker, J. N.; Hall, W. P.; Lyandres, O.; Shah, N. C.; Zhao, J.; Van Duyne, R. P., Biosensing with plasmonic nanosensors. *Nat. Mater*. **2008**, 7, 442-453.

2. Zhou, X.; Xu, W.; Liu, G.; Panda, D.; Chen, P., Size-Dependent Catalytic Activity and Dynamics of Gold Nanoparticles at the Single-Molecule Level. *J. Am. Chem. Soc.* **2010**, 132, 138-146.

3. Yuan, Y.; Yan, N.; Dyson, P. J., pH-Sensitive Gold Nanoparticle Catalysts for the Aerobic Oxidation of Alcohols. *Inorg. Chem*. **2011**, 50, 11069-11074.

4. Cong, H.; Becker, C. F.; Elliott, S. J.; Grinstaff, M. W.; Porco, J. A., Silver Nanoparticle-Catalyzed Diels−Alder Cycloadditions of 2′-Hydroxychalcones. *J. Am. Chem. Soc.* **2010**, 132, 7514-7518.

5. Ghosh, P.; Han, G.; De, M.; Kim, C. K.; Rotello, V. M., Gold nanoparticles in delivery applications. *Adv. Drug Deliv. Rev*. **2008**, 60, 1307-1315.

6. Benyettou, F.; Rezgui, R.; Ravaux, F.; Jaber, T.; Blumer, K.; Jouiad, M.; Motte, L.; Olsen, J. C.; Platas-Iglesias, C.; Magzoub, M.; Trabolsi, A., Synthesis of silver nanoparticles for the dual delivery of doxorubicin and alendronate to cancer cells. *J. Mater. Chem. B*. **2015**, 3, 7237-7245.

7. Chou, C.-H.; Chen, F.-C., Plasmonic nanostructures for light trapping in organic photovoltaic devices. *Nanoscale* **2014**, 6, 8444-8458.

8. Atwater, H. A.; Polman, A., Plasmonics for improved photovoltaic devices. *Nat. Mater.* **2010**, 9, 205-213.

9. Tian, Z.-Q.; Ren, B.; Wu, D.-Y., Surface-Enhanced Raman Scattering: From Noble to Transition Metals and from Rough Surfaces to Ordered Nanostructures. *J. Phys. Chem. B* **2002**, 106, 9463-9483.

10. Shen, C.; Hui, C.; Yang, T.; Xiao, C.; Tian, J.; Bao, L.; Chen, S.; Ding, H.; Gao, H., Monodisperse Noble-Metal Nanoparticles and Their Surface Enhanced Raman Scattering Properties. *Chem. Mater*. **2008**, 20, 6939-6944.

11. Yang, X.; Yang, M.; Pang, B.; Vara, M.; Xia, Y., Gold Nanomaterials at Work in Biomedicine. *Chem. Rev*. **2015**, 115, 10410-10488.

12. Eustis, S.; El-Sayed, M. A., Why gold nanoparticles are more precious than pretty gold: Noble metal surface plasmon resonance and its enhancement of the radiative and nonradiative properties of nanocrystals of different shapes. *Chem. Soc. Rev*. **2006**, 35, 209-217.

13. Turkevich, J.; Stevenson, P. C.; Hillier, J., A study of the nucleation and growth processes in the synthesis of colloidal gold. *Discuss. Faraday Soc*. **1951**, 11, 55-75.

14. Frens, G., Controlled Nucleation for the Regulation of the Particle Size in Monodisperse Gold Suspensions. *Nature Phys. Sci*. **1973**, 241, 20-22.

15. Dreaden, E. C.; Alkilany, A. M.; Huang, X.; Murphy, C. J.; El-Sayed, M. A., The golden age: gold nanoparticles for biomedicine. *Chem. Soc. Rev*. **2012**, 41, 2740-2779.

16. Brust, M.; Walker, M.; Bethell, D.; Schiffrin, D. J.; Whyman, R., Synthesis of thiol-derivatised gold nanoparticles in a two-phase Liquid-Liquid system. *J. Chem. Soc., Chem. Commun*. **1994**, 801-802.

17. Daniel, M.-C.; Astruc, D., Gold Nanoparticles: Assembly, Supramolecular Chemistry, Quantum-Size-Related Properties, and Applications toward Biology, Catalysis, and Nanotechnology. *Chem. Rev*. **2004**, 104, 293-346.

18. Lee, P. C.; Meisel, D., Adsorption and surface-enhanced Raman of dyes on silver and gold sols. *J. Phys. Chem*. **1982**, 86, 3391-3395.

19. Pillai, Z. S.; Kamat, P. V., What Factors Control the Size and Shape of Silver Nanoparticles in the Citrate Ion Reduction Method? *J. Phys. Chem. B* **2004**, 108, 945-951.

20. Henglein, A.; Giersig, M., Formation of Colloidal Silver Nanoparticles: Capping Action of Citrate. *J. Phys. Chem. B* **1999**, 103, 9533-9539.

21. Love, J. C.; Estroff, L. A.; Kriebel, J. K.; Nuzzo, R. G.; Whitesides, G. M., Self-Assembled Monolayers of Thiolates on Metals as a Form of Nanotechnology. *Chem. Rev*. **2005**, 105, 1103-1170.

22. Lin, S.-Y.; Tsai, Y.-T.; Chen, C.-C.; Lin, C.-M.; Chen, C.-h., Two-Step Functionalization of Neutral and Positively Charged Thiols onto Citrate-Stabilized Au Nanoparticles. *J. Phys. Chem. B* **2004**, 108, 2134-2139.

23. Sung, K.-M.; Mosley, D. W.; Peelle, B. R.; Zhang, S.; Jacobson, J. M., Synthesis of Monofunctionalized Gold Nanoparticles by Fmoc Solid-Phase Reactions. *J. Am. Chem. Soc.* **2004**, 126, 5064-5065.

24. Ulman, A., Formation and Structure of Self-Assembled Monolayers. *Chem. Rev.* **1996**, 96, 1533-1554.

25. Dannenberger, O.; Buck, M.; Grunze, M., Self-Assembly of n-Alkanethiols: A Kinetic Study by Second Harmonic Generation. *J. Phys. Chem. B* **1999**, 103, 2202-2213.

26. Laibinis, P. E.; Fox, M. A.; Folkers, J. P.; Whitesides, G. M., Comparisons of self-assembled monolayers on silver and gold: mixed monolayers derived from $HS(CH_2)_{21}X$ and $HS(CH_2)_{10}Y$ (X, Y = CH_3, CH_2OH) have similar properties. *Langmuir* **1991**, 7, 3167-3173.

27. Laibinis, P. E.; Whitesides, G. M.; Allara, D. L.; Tao, Y. T.; Parikh, A. N.; Nuzzo, R. G., Comparison of the structures and wetting properties of self-assembled monolayers of n-alkanethiols on the coinage metal surfaces, copper, silver, and gold. *J. Am. Chem. Soc*. **1991**, 113, 7152-7167.

28. Laibinis, P. E.; Whitesides, G. M., .omega.-Terminated alkanethiolate monolayers on surfaces of copper, silver, and gold have similar wettabilities. *J. Am. Chem. Soc.* **1992**, 114, 1990-1995.

29. Walczak, M. M.; Chung, C.; Stole, S. M.; Widrig, C. A.; Porter, M. D., Structure and interfacial properties of spontaneously adsorbed n-alkanethiolate monolayers on evaporated silver surfaces. *J. Am. Chem. Soc*. **1991**, 113, 2370-2378.

30. Weeraman, C.; Yatawara, A. K.; Bordenyuk, A. N.; Benderskii, A. V., Effect of Nanoscale Geometry on Molecular Conformation: Vibrational Sum-Frequency Generation of Alkanethiols on Gold Nanoparticles. *J. Am. Chem. Soc*. **2006**, 128, 14244-14245.

31. Levin, C. S.; Janesko, B. G.; Bardhan, R.; Scuseria, G. E.; Hartgerink, J. D.; Halas, N. J., Chain-Length-Dependent Vibrational Resonances in Alkanethiol Self-Assembled Monolayers Observed on Plasmonic Nanoparticle Substrates. *Nano Lett*. **2006**, 6, 2617-2621.

32. Chen, C.-F.; Tzeng, S.-D.; Chen, H.-Y.; Lin, K.-J.; Gwo, S., Tunable Plasmonic Response from Alkanethiolate-Stabilized Gold Nanoparticle Superlattices: Evidence of Near-Field Coupling. *J. Am. Chem. Soc*. **2008**, 130, 824-826.

33. Vericat, C.; Vela, M. E.; Salvarezza, R. C., Self-assembled monolayers of alkanethiols on Au(111): surface structures, defects and dynamics. *Phys. Chem. Chem. Phys.* **2005**, 7, 3258-3268.

34. Akkerman, H. B.; Blom, P. W. M.; de Leeuw, D. M.; de Boer, B., Towards molecular electronics with large-area molecular junctions. *Nature* **2006**, 441, 69-72.

35. Bruot, C.; Hihath, J.; Tao, N., Mechanically controlled molecular orbital alignment in single molecule junctions. *Nat. Nano* **2012**, 7, 35-40.

36. Izquierdo-Lorenzo, I.; Kubackova, J.; Manchon, D.; Mosset, A.; Cottancin, E.; Sanchez-Cortes, S., Linking Ag Nanoparticles by Aliphatic α,ω-Dithiols: A Study of the Aggregation and Formation of Interparticle Hot Spots. *J. Phys. Chem. C* **2013**, 117, 16203-16212.

37. Vericat, C.; Vela, M. E.; Benitez, G.; Carro, P.; Salvarezza, R. C., Self-assembled monolayers of thiols and dithiols on gold: new challenges for a well-known system. *Chem. Soc. Rev*. **2010**, 39, 1805-1834.

38. Jia, J.; Mukherjee, S.; Hamoudi, H.; Nannarone, S.; Pasquali, L.; Esaulov, V. A., Lying-Down to Standing-Up Transitions in Self Assembly of Butanedithiol Monolayers on Gold and Substitutional Assembly by Octanethiols. *J. Phys. Chem. C* **2013**, 117, 4625-4631.

39. Rieley, H.; Kendall, G. K.; Zemicael, F. W.; Smith, T. L.; Yang, S., X-ray Studies of Self-Assembled Monolayers on Coinage Metals. 1. Alignment and Photooxidation in 1,8-Octanedithiol and 1-Octanethiol on Au. *Langmuir* **1998**, 14, 5147-5153.

40. Pugmire, D. L.; Tarlov, M. J.; van Zee, R. D.; Naciri, J., Structure of 1,4-Benzenedimethanethiol Self-Assembled Monolayers on Gold Grown by Solution and Vapor Techniques. *Langmuir* **2003**, 19, 3720-3726.

41. Stammer, X.; Tonigold, K.; Bashir, A.; Kafer, D.; Shekhah, O.; Hulsbusch, C.; Kind, M.; Gro; Woll, C., A highly ordered, aromatic bidentate self-assembled monolayer on Au(111): a combined experimental and theoretical study. *Phys. Chem. Chem. Phys*. **2010**, 12, 6445-6454.

42. Cometto, F. P.; Ruano, G.; Ascolani, H.; Zampieri, G., Adlayers of Alkanedithiols on Au(111): Effect of Disulfide Reducing Agent. *Langmuir* **2013**, 29, 1400-1406.

43. Kohli, P.; Taylor, K. K.; Harris, J. J.; Blanchard, G. J., Assembly of Covalently-Coupled Disulfide Multilayers on Gold. *J. Am. Chem. Soc*. **1998**, 120, 11962-11968.

44. Pasquali, L.; Terzi, F.; Zanardi, C.; Pigani, L.; Seeber, R.; Paolicelli, G.; Suturin, S. M.; Mahne, N.; Nannarone, S., Structure and properties of 1,4-benzenedimethanethiol films grown from solution on Au(1 1 1): An XPS and NEXAFS study. *Surf. Sci*. **2007**, 601, 1419-1427.

45. Jia, J.; Giglia, A.; Flores, M.; Grizzi, O.; Pasquali, L.; Esaulov, V. A., 1,4-Benzenedimethanethiol Interaction with Au(110), Ag(111), Cu(100), and Cu(111) Surfaces: Self-Assembly and Dissociation Processes. *J. Phys. Chem. C* **2014**, 118, 26866-26876.

46. Garg, N.; Lee, T. R., Self-Assembled Monolayers Based on Chelating Aromatic Dithiols on Gold. *Langmuir* **1998**, 14, 3815-3819.

47. Lee, Y. J.; Jeon, I. C.; Paik, W.-k.; Kim, K., Self-Assembly of 1,2-Benzenedithiol on Gold and Silver: Fourier Transform Infrared Spectroscopy and Quartz Crystal Microbalance Study. *Langmuir* **1996**, 12, 5830-5837.

48. Lim, J. K.; Kim, Y.; Kwon, O.; Joo, S.-W., Adsorption of 1,3-Benzenedithiol and 1,3-Benzenedimethanethiol on Gold Surfaces. *ChemPhysChem* **2008**, 9, 1781-1787.

49. Salazar Alarcón, L.; Cristina, L. J.; Shen, J.; Jia, J.; Esaulov, V. A.; Sánchez, E. A.; Grizzi, O., Growth of 1,4-Benzenedimethanethiol Films on Au, Ag, and Cu: Effect of Surface Temperature on the Adsorption Kinetics and on the Single versus Multilayer Formation. *J. Phys. Chem. C* **2013**, 117, 17521-17530.

50. Alarcón, L. S.; Chen, L.; Esaulov, V. A.; Gayone, J. E.; Sánchez, E. A.; Grizzi, O., Thiol Terminated 1,4-Benzenedimethanethiol Self-Assembled Monolayers on Au(111) and InP(110) from Vapor Phase. *J. Phys. Chem. C* **2010**, 114, 19993-19999.

51. Hamoudi, H.; Prato, M.; Dablemont, C.; Cavalleri, O.; Canepa, M.; Esaulov, V. A., Self-Assembly of 1,4-Benzenedimethanethiol Self-Assembled Monolayers on Gold. *Langmuir* **2010**, 26, 7242-7247.

52. Pasquali, L.; Terzi, F.; Seeber, R.; Nannarone, S.; Datta, D.; Dablemont, C.; Hamoudi, H.; Canepa, M.; Esaulov, V. A., UPS, XPS, and NEXAFS Study of Self-Assembly of Standing 1,4-Benzenedimethanethiol SAMs on Gold. *Langmuir* **2011**, 27, 4713-4720.

53. Joo, S. W.; Han, S. W.; Kim, K., Adsorption Characteristics of p-Xylene-α,α‘-dithiol on Gold and Silver Surfaces: Surface-Enhanced Raman Scattering and Ellipsometry Study. *J. Phys. Chem. B* **1999**, 103, 10831-10837.

54. Joo, S. W.; Han, S. W.; Kim, K., Multilayer Formation of 1,2-Ethanedithiol on Gold: Surface-Enhanced Raman Scattering and Ellipsometry Study. *Langmuir* **2000**, 16, 5391-5396.

55. Cho, S. H.; Han, H. S.; Jang, D.-J.; Kim, K.; Kim, M. S., Raman Spectroscopic Study of 1,4-Benzenedithiol Adsorbed on Silver. *J. Phys. Chem*. **1995**, 99, 10594-10599.

56. Lee, T. G.; Kim, K.; Kim, M. S., Adsorption of xylene-.alpha.,.alpha.'-dithiol on silver investigated by Raman spectroscopy. *J. Phys. Chem*. **1991**, 95, 9950-9955.

57. Venkataramanan, M.; Ma, S.; Pradeep, T., 3D Monolayers of 1,4-Benzenedimethanethiol on Au and Ag Clusters: Distinct Difference in Adsorption Geometry with the Corresponding 2D Monolayers. *J. Colloid Interface Sci*. **1999**, 216, 134-142.

58. Heister, K.; Zharnikov, M.; Grunze, M.; Johansson, L. S. O.; Ulman, A., Characterization of X-ray Induced Damage in Alkanethiolate Monolayers by High-Resolution Photoelectron Spectroscopy. *Langmuir* **2001**, 17, 8-11.

59. Jäger, B.; Schürmann, H.; Müller, H. U.; Himmel, H.-J.; Neumann, M.; Grunze, M.; Wöll, C., X-ray and Low Energy Electron Induced Damage in Alkanethiolate Monolayers on Au-substrates. *Z. Phys. Chem*. **1997**, 202, 263-272.

60. Greenler, R. G.; Snider, D. R.; Witt, D.; Sorbello, R. S., The metal-surface selection rule for infrared spectra of molecules adsorbed on small metal particles. *Surf. Sci*. **1982**, 118, 415-428.

61. Johnson, E.; Aroca, R., Surface-enhanced infrared spectroscopy of monolayers. *J. Phys. Chem*. **1995**, 99, 9325-9330.

62. Moskovits, M., Surface selection rules. *J. Chem. Phys*. **1982**, 77, 4408-4416.

63. Moskovits, M., Surface-enhanced spectroscopy. *Rev. Mod. Phys*. **1985**, 57, 783-826.

64. Haynes, C. L.; McFarland, A. D.; Duyne, R. P. V., Surface-Enhanced Raman Spectroscopy. *Anal. Chem*. **2005**, 77, 338 A-346 A.

65. Kelly, K. L.; Coronado, E.; Zhao, L. L.; Schatz, G. C., The Optical Properties of Metal Nanoparticles: The Influence of Size, Shape, and Dielectric Environment. *J. Phys. Chem. B* **2003**, 107, 668-677.

66. Miller, M. M.; Lazarides, A. A., Sensitivity of Metal Nanoparticle Surface Plasmon Resonance to the Dielectric Environment. *J. Phys. Chem. B* **2005**, 109, 21556-21565.

67. Jain, P. K.; Huang, X.; El-Sayed, I. H.; El-Sayed, M. A., Noble Metals on the Nanoscale: Optical and Photothermal Properties and Some Applications in Imaging, Sensing, Biology, and Medicine. *Acc. Chem. Res*. **2008**, 41, 1578-1586.

68. Willets, K. A.; Duyne, R. P. V., Localized Surface Plasmon Resonance Spectroscopy and Sensing. *Annu. Rev. Phys. Chem*. **2007**, 58, 267-297.

69. El-Sayed, M. A., Some Interesting Properties of Metals Confined in Time and Nanometer Space of Different Shapes. *Acc. Chem. Res*. **2001**, 34, 257-264.

70. Mock, J. J.; Barbic, M.; Smith, D. R.; Schultz, D. A.; Schultz, S., Shape effects in plasmon resonance of individual colloidal silver nanoparticles. *J. Chem. Phys*. **2002**, 116, 6755-6759.

71. Mie, G., Beiträge zur Optik trüber Medien, speziell kolloidaler Metallösungen. *Annalen der Physik* **1908**, 330 (3), 377-445.

72. Mulvaney, P., Surface Plasmon Spectroscopy of Nanosized Metal Particles. *Langmuir* **1996**, 12, 788-800.

73. Saha, K.; Agasti, S. S.; Kim, C.; Li, X.; Rotello, V. M., Gold Nanoparticles in Chemical and Biological Sensing. *Chem. Rev*. **2012**, 112, 2739-2779.

74. Lee, H. M.; Jin, S. M.; Kim, H. M.; Suh, Y. D., Single-molecule surface-enhanced Raman spectroscopy: a perspective on the current status. *Phys. Chem. Chem. Phys*. **2013**, 15, 5276-5287.

75. Ru, E. C. L.; Etchegoin, P. G., Single-Molecule Surface-Enhanced Raman Spectroscopy. *Annu. Rev. Phys. Chem*. **2012**, 63, 65-87.

76. Campion, A.; Kambhampati, P., Surface-enhanced Raman scattering. *Chem. Soc. Rev*. **1998**, 27, 241-250.

77. Lombardi, J. R.; Birke, R. L.; Lu, T.; Xu, J., Charge-transfer theory of surface enhanced Raman spectroscopy: Herzberg–Teller contributions. *J. Chem. Phys*. **1986**, 84, 4174-4180.

78. Arenas, J. F.; Fernández, D. J.; Soto, J.; López-Tocón, I.; Otero, J. C., Role of the Electrode Potential in the Charge-Transfer Mechanism of Surface-Enhanced Raman Scattering. *J. Phys. Chem. B* **2003**, 107, 13143-13149.

79. Farcau, C.; Astilean, S., Mapping the SERS Efficiency and Hot-Spots Localization on Gold Film over Nanospheres Substrates. *J. Phys. Chem. C* **2010**, 114, 11717-11722.

80. Tan, A.; Balachandran, J.; Sadat, S.; Gavini, V.; Dunietz, B. D.; Jang, S.-Y.; Reddy, P., Effect of Length and Contact Chemistry on the Electronic Structure and Thermoelectric Properties of Molecular Junctions. *J. Am. Chem. Soc.* **2011**, 133, 8838-8841.

81. Reddy, P.; Jang, S.-Y.; Segalman, R. A.; Majumdar, A., Thermoelectricity in Molecular Junctions. *Science* **2007**, 315, 1568-1571.

82. Reed, M. A.; Zhou, C.; Muller, C. J.; Burgin, T. P.; Tour, J. M., Conductance of a Molecular Junction. *Science* **1997**, 278, 252-254.

83. Nitzan, A.; Ratner, M. A., Electron Transport in Molecular Wire Junctions. *Science* **2003**, 300, 1384-1389.

84. El-Khoury, P. Z.; Hu, D.; Apkarian, V. A.; Hess, W. P., Raman Scattering at Plasmonic Junctions Shorted by Conductive Molecular Bridges. *Nano Lett*. **2013**, 13, 1858-1861.

85. Cui, L.; Liu, B.; Vonlanthen, D.; Mayor, M.; Fu, Y.; Li, J.-F.; Wandlowski, T., In Situ Gap-Mode Raman Spectroscopy on Single-Crystal Au(100) Electrodes: Tuning the Torsion Angle of 4,4'-Biphenyldithiols by an Electrochemical Gate Field. *J. Am. Chem. Soc*. **2011**, 133, 7332-7335.

86. Wang, X.; Li, M.; Meng, L.; Lin, K.; Feng, J.; Huang, T.; Yang, Z.; Ren, B., Probing the Location of Hot Spots by Surface-Enhanced Raman Spectroscopy: Toward Uniform Substrates. *ACS Nano* **2013**, 8, 528-536.

87. Banik, M.; Nag, A.; El-Khoury, P. Z.; Rodriguez, P. A.; Guarrotxena, N.; Bazan, G. C.; Apkarian, V. A., Surface-Enhanced Raman Scattering of a Single Nanodumbbell: Dibenzyldithio-Linked Silver Nanospheres. *J. Phys. Chem. C* **2012**, 116, 10415-10423.

88. Banik, M.; El-Khoury, P. Z.; Nag, A.; Rodriguez-Perez, A.; Guarrottxena, N.; Bazan, G. C.; Apkarian, V. A., Surface-Enhanced Raman Trajectories on a Nano-Dumbbell: Transition from Field to Charge Transfer Plasmons as the Spheres Fuse. *ACS Nano* **2012**, 6, 10343-10354.

89. Tan, S. F.; Wu, L.; Yang, J. K. W.; Bai, P.; Bosman, M.; Nijhuis, C. A., Quantum Plasmon Resonances Controlled by Molecular Tunnel Junctions. *Science* **2014**, 343, 1496-1499.

90. Osberg, K. D.; Rycenga, M.; Harris, N.; Schmucker, A. L.; Langille, M. R.; Schatz, G. C.; Mirkin, C. A., Dispersible Gold Nanorod Dimers with Sub-5 nm Gaps as Local Amplifiers for Surface-Enhanced Raman Scattering. *Nano Lett*. **2012**, 12, 3828-3832.

91. Joo, S. W.; Han, S. W.; Kim, K., Adsorption of 1,4-Benzenedithiol on Gold and Silver Surfaces: Surface-Enhanced Raman Scattering Study. *J. Colloid Interface Sci.* **2001**, 240, 391-399.

92. Zhang, D.; Xie, Y.; Mrozek, M. F.; Ortiz, C.; Davisson, V. J.; Ben-Amotz, D., Raman Detection of Proteomic Analytes. *Anal. Chem*. **2003**, 75, 5703-5709.

93. Zhang, D.; Ansar, S. M., Ratiometric Surface Enhanced Raman Quantification of Ligand Adsorption onto a Gold Nanoparticle. *Anal. Chem*. **2010**, 82, 5910-5914.

94. Freeman, R. G.; Hommer, M. B.; Grabar, K. C.; Jackson, M. A.; Natan, M. J., Ag-Clad Au Nanoparticles: Novel Aggregation, Optical, and Surface-Enhanced Raman Scattering Properties. *J. Phys. Chem*. **1996**, 100, 718-724.

95. Jin, R.; Wu, G.; Li, Z.; Mirkin, C. A.; Schatz, G. C., What Controls the Melting Properties of DNA-Linked Gold Nanoparticle Assemblies? *J. Am. Chem. Soc*. **2003**, 125, 1643-1654.

96. Englebienne, P., Use of colloidal gold surface plasmon resonance peak shift to infer affinity constants from the interactions between protein antigens and antibodies specific for single or multiple epitopes. *Analyst* **1998**, 123, 1599-1603.

97. Eck, D.; Helm, C. A.; Wagner, N. J.; Vaynberg, K. A., Plasmon Resonance Measurements of the Adsorption and Adsorption Kinetics of a Biopolymer onto Gold Nanocolloids. *Langmuir* **2001**, 17, 957-960.

98. Sun, Y.; Xia, Y., Increased Sensitivity of Surface Plasmon Resonance of Gold Nanoshells Compared to That of Gold Solid Colloids in Response to Environmental Changes. *Anal. Chem*. **2002**, 74, 5297-5305.

99. Siriwardana, K.; Gadogbe, M.; Ansar, S. M.; Vasquez, E. S.; Collier, W. E.; Zou, S.; Walters, K. B.; Zhang, D., Ligand Adsorption and Exchange on Pegylated Gold Nanoparticles. *J. Phys. Chem. C* **2014**, 118, 11111-11119.

100. Ansar, S. M.; Ameer, F. S.; Hu, W.; Zou, S.; Pittman, C. U.; Zhang, D., Removal of Molecular Adsorbates on Gold Nanoparticles Using Sodium Borohydride in Water. *Nano Lett*. **2013**, 13, 1226-1229.

101. Ansar, S. M.; Perera, G. S.; Jiang, D.; Holler, R. A.; Zhang, D., Organothiols Self-Assembled Onto Gold: Evidence for Deprotonation of the Sulfur-Bound Hydrogen and Charge-Transfer from Thiolate. *J. Phys. Chem. C* **2013**, 117, 8793-8798.

102. Ansar, S. M.; Perera, G. S.; Gomez, P.; Salomon, G.; Vasquez, E. S.; Chu, I. W.; Zou, S.; Pittman, C. U.; Walters, K. B.; Zhang, D., Mechanistic Study of Continuous Reactive Aromatic Organothiol Adsorption onto Silver Nanoparticles. *J. Phys. Chem. C* **2013**, 117, 27146-27154.

103. Siriwardana, K.; Wang, A.; Gadogbe, M.; Collier, W. E.; Fitzkee, N. C.; Zhang, D., Studying the Effects of Cysteine Residues on Protein Interactions with Silver Nanoparticles. *J. Phys. Chem. C* **2015**, 119, 2910-2916.

104. Siriwardana, K.; Wang, A.; Vangala, K.; Fitzkee, N.; Zhang, D., Probing the Effects of Cysteine Residues on Protein Adsorption onto Gold Nanoparticles Using Wild-Type and Mutated GB3 Proteins. *Langmuir* **2013**, 29, 10990-10996.

105. Gadogbe, M.; Ansar, S. M.; Chu, I. W.; Zou, S.; Zhang, D., Comparative Study of the Self-Assembly of Gold and Silver Nanoparticles onto Thiophene Oil. *Langmuir* **2014**, 30, 11520-11527.

106. Yoon, J. H.; Zhou, Y.; Blaber, M. G.; Schatz, G. C.; Yoon, S., Surface Plasmon Coupling of Compositionally Heterogeneous Core–Satellite Nanoassemblies. *J. Phys. Chem. Lett*. **2013**, 4, 1371-1378.

107. Cha, H.; Yoon, J. H.; Yoon, S., Probing Quantum Plasmon Coupling Using Gold Nanoparticle Dimers with Tunable Interparticle Distances Down to the Subnanometer Range. *ACS Nano* **2014**, 8, 8554-8563.

108. Yoon, J. H.; Lim, J.; Yoon, S., Controlled Assembly and Plasmonic Properties of Asymmetric Core–Satellite Nanoassemblies. *ACS Nano* **2012**, 6, 7199-7208.

109. Akkerman, H. B.; Naber, R. C. G.; Jongbloed, B.; van Hal, P. A.; Blom, P. W. M.; de Leeuw, D. M.; de Boer, B., Electron tunneling through alkanedithiol self-assembled monolayers in large-area molecular junctions. *PNAS* **2007**, 104, 11161-11166.

110. Cui, X. D.; Primak, A.; Zarate, X.; Tomfohr, J.; Sankey, O. F.; Moore, A. L.; Moore, T. A.; Gust, D.; Harris, G.; Lindsay, S. M., Reproducible Measurement of Single-Molecule Conductivity. *Science* **2001**, 294, 571-574.

111. Akkerman, H. B.; Kronemeijer, A. J.; van Hal, P. A.; de Leeuw, D. M.; Blom, P. W. M.; de Boer, B., Self-Assembled-Monolayer Formation of Long Alkanedithiols in Molecular Junctions. *Small* **2008**, 4, 100-104.

112. Kubackova, J.; Fabriciova, G.; Miskovsky, P.; Jancura, D.; Sanchez-Cortes, S., Sensitive Surface-Enhanced Raman Spectroscopy (SERS) Detection of Organochlorine Pesticides by Alkyl Dithiol-Functionalized Metal Nanoparticles-Induced Plasmonic Hot Spots. *Anal. Chem*. **2015**, 87, 663-669.

113. Joo, S. W.; Han, S. W.; Kim, K., Adsorption characteristics of 1,3-propanedithiol on gold. Surface-enhanced Raman scattering and ellipsometry study. *J. Phys. Chem. B* **2000**, 104, 6218-6224.

114. Gadogbe, M.; Chen, M.; Zhao, X.; Saebo, S.; Beard, D. J.; Zhang, D., Can Para-Aryl-Dithiols Cross-Link Two Plasmonic Noble Nanoparticles as Monolayer Dithiolate Spacers? *J. Phys. Chem. C* **2015**, 119, 6626-6633.

115. Leung, T. Y. B.; Gerstenberg, M. C.; Lavrich, D. J.; Scoles, G.; Schreiber, F.; Poirier, G. E., 1,6-Hexanedithiol Monolayers on Au(111): A Multitechnique Structural Study. *Langmuir* **1999**, 16, 549-561.

116. Kobayashi, K.; Yamada, H.; Horiuchi, T.; Matsushige, K., UHV-STM studies on the structures of alkanedithiol self-assembled monolayers. *Appl. Surf. Sci*. **1999**, 144–145, 435-438.

117. Carot, M. L.; Esplandiu, M. J.; Cometto, F. P.; Patrito, E. M.; Macagno, V. A., Reactivity of 1,8-octanedithiol monolayers on Au(111): Experimental and theoretical investigation. *J. Electroanal. Chem*. **2005**, 579, 13-23.

118. Millone, M. a. A. D.; Hamoudi, H.; Rodríguez, L.; Rubert, A.; Benítez, G. A.; Vela, M. a. E.; Salvarezza, R. C.; Gayone, J. E.; Sánchez, E. A.; Grizzi, O.; Dablemont, C. l.; Esaulov, V. A., Self-Assembly of Alkanedithiols on Au(111) from Solution: Effect of Chain Length and Self-Assembly Conditions. *Langmuir* **2009**, 25, 12945-12953.

119. Cometto, F. P.; Calderón, C. A.; Euti, E. M.; Jacquelín, D. K.; Pérez, M. A.; Patrito, E. M.; Macagno, V. A., Electrochemical study of adlayers of α,ω-alkanedithiols on Au(111): Influence of the forming solution, chain length and treatment with mild reducing agents. *J. Electroanal. Chem*. **2011**, 661, 90-99.

120. Hamoudi, H.; Guo, Z.; Prato, M.; Dablemont, C.; Zheng, W. Q.; Bourguignon, B.; Canepa, M.; Esaulov, V. A., On the self assembly of short chain alkanedithiols. *Phys. Chem. Chem. Phys*. **2008**, 10, 6836-6841.

121. Dhirani, A.; Hines, M. A.; Fisher, A. J.; Ismail, O.; Guyot-Sionnest, P., Structure of Self-Assembled Decanethiol on Ag(111): A Molecular Resolution Scanning Tunneling Microscopy Study. *Langmuir* **1995**, 11, 2609-2614.

122. Hong, Y.-K.; Yu, H.; Lee, T. G.; Lee, N.; Bahng, J. H.; Song, N. W.; Chegal, W.; Shon, H. K.; Koo, J.-Y., Highly-ordered self-assembled monolayer of alkanethiol on thermally annealed polycrystalline gold films. *Chem. Phys*. **2014**, 428, 105-110.

123. Ansar, S. M.; Gadogbe, M.; Siriwardana, K.; Howe, J. Y.; Dogel, S.; Hosseinkhannazer, H.; Collier, W. E.; Rodriguez, J.; Zou, S.; Zhang, D., Dispersion Stability, Ligand Structure and Conformation, and SERS Activities of 1-Alkanethiol Functionalized Gold and Silver Nanoparticles. *J. Phys. Chem. C* **2014**, 118, 24925-24934.

124. Schlücker, S., Surface-Enhanced Raman Spectroscopy: Concepts and Chemical Applications. *Angew. Chem. Int. Ed*. **2014**, 53, 4756-4795.

125. Moskovits, M., Surface-enhanced Raman spectroscopy: a brief retrospective. *J. Raman Spectrosc.* **2005**, 36, 485-496.

126. Mishchenko, M. I.; Travis, L. D.; Mackowski, D. W., T-matrix computations of light scattering by nonspherical particles: A review. *J. Quant. Spectrosc. Radiat. Transfer.* **1996**, 55, 535-575.

127. Weisbecker, C. S.; Merritt, M. V.; Whitesides, G. M., Molecular Self-Assembly of Aliphatic Thiols on Gold Colloids. *Langmuir* **1996**, 12, 3763-3772.

128. Fenter, P.; Eberhardt, A.; Eisenberger, P., Self-Assembly of n-Alkyl Thiols as Disulfides on Au(111). *Science* **1994**, 266, 1216-1218.

129. Ansar, S. M.; Haputhanthri, R.; Edmonds, B.; Liu, D.; Yu, L.; Sygula, A.; Zhang, D., Determination of the Binding Affinity, Packing, and Conformation of Thiolate and Thione Ligands on Gold Nanoparticles. *J. Phys. Chem. C* **2010**, 115, 653-660.

130. Storhoff, J. J.; Lazarides, A. A.; Mucic, R. C.; Mirkin, C. A.; Letsinger, R. L.; Schatz, G. C., What Controls the Optical Properties of DNA-Linked Gold Nanoparticle Assemblies? *J. Am. Chem. Soc*. **2000**, 122, 4640-4650.

131. Jain, P. K.; Huang, W.; El-Sayed, M. A., On the Universal Scaling Behavior of the Distance Decay of Plasmon Coupling in Metal Nanoparticle Pairs: A Plasmon Ruler Equation. *Nano Lett*. **2007**, 7, 2080-2088.

132. Reinhard, B. M.; Siu, M.; Agarwal, H.; Alivisatos, A. P.; Liphardt, J., Calibration of Dynamic Molecular Rulers Based on Plasmon Coupling between Gold Nanoparticles. *Nano Lett*. **2005**, 5, 2246-2252.

133. Sonnichsen, C.; Reinhard, B. M.; Liphardt, J.; Alivisatos, A. P., A molecular ruler based on plasmon coupling of single gold and silver nanoparticles. *Nat. Biotech*. **2005**, 23, 741-745.